Projected changes in forest fire season, number of fires and burnt area in Fennoscandia by 2100

Outi Kinnunen[1], Leif Backman[1], Juha Aalto[2,3], Tuula Aalto[1], and Tiina Markkanen[1]

[1]Climate Research, Finnish Meteorological Institute, Erik Palménin aukio 1, 00560 Helsinki, Finland.
[2]Weather and Climate Change Impact Research, Finnish Meteorological Institute, Erik Palménin aukio 1, 00560 Helsinki, Finland.
[3]Department of Geosciences and Geography, University of Helsinki, P.O. Box 64, Gustaf Hällströmin katu 2a, 00560 Helsinki, Finland

Correspondence: Outi Kinnunen (outi.kinnunen@fmi.fi)

Abstract. Forest fire dynamics are expected to alter due to climate change. Despite the projected increase in precipitation, rising temperatures will amplify forest fire risk from the present to the end of the century. Here, we analysed the changes in fire season, number of fires and burnt area in Fennoscandia from 1951 to 2100. The JSBACH-SPITFIRE ecosystem model regional simulations were done under two climate change forcing scenarios (RCP 4.5 and RCP 8.5) and three global climate driver models (CanESM2, CNRM-CM5 and MIROC5) with a 0.5° resolution. Simulations were forced by downscaled and bias-corrected EURO-CORDEX data. Generally, as a consequence of the projected longer fire season and drier fuel, the probability of fires is projected to increase. However, changes in fire season, number of fires and burnt area are highly dependent on the climate projection and location. The fire season is estimated to increase on average from (20 ± 7) days to (52 ± 12) days, starting from (10 ± 9) days to (23 ± 11) days earlier and ending from (10 ± 10) days to (30 ± 16) days later, compared to the reference period (1981–2010) by the end of the century (2071–2100). The results for Finland indicate a change in the number of fires ranging from $(-7 \pm 4)\%$ to (98 ± 56) % and a change in the burnt area ranging from (-19 ± 24) % to (87 ± 42) %. These findings contribute to a better understanding of potential changes in the future fire seasons in Northern Europe.

1 Introduction

Forest fires are natural to boreal ecosystems. Historically, forest fires are one of the primary disturbances in Fennoscandia, (Engelmark, 1999; Ramberg et al., 2018; Tolonen and Pitkänen, 2004), where the forests are dominated by Scots pine and Norway spruce. Nowadays, due to efficient fire monitoring and suppression, fire is a relatively rare event in Fennoscandia (Ramberg, 2020; Vajda et al., 2014). For example, on average, only 0.006 % (less than 2000 ha) of Swedish forests burn per year, although in the exceptionally dry summer of 2018, there was a high number of forest fires (Ramberg et al., 2018). In Finland, the annual burnt area is 500–600 ha (Aalto and Venäläinen, 2021). Nevertheless, Lehtonen et al. (2016) pointed out

that the number of large forest fires (> 10 ha) may even triple during the present century. Furthermore, in the Siberian Arctic, an almost exponential increase has been observed in burnt areas (Descals et al., 2022). Today, population density, landscape patterns, prescribed fires, and fire prevention policies strongly influence forest fires (Flannigan et al., 2009; Larjavaara et al., 2005a). The only natural cause of fires is lightning (Larjavaara et al., 2005b; Gromtsev, 2002), and fires are mainly ignited, about 90 % in Finland (Mäkelä, 2015; Kilpeläinen et al., 2010), by human actions (Flannigan et al., 2009; Ramberg, 2020; Hantson et al., 2015). The population density is low in Finland, and fires are more likely to occur in the more densely populated southern part than in the northern part of the country (Vajda et al., 2014; Larjavaara et al., 2005a).

Forest fires have a multitude of impacts on the ecosystem and climate. Fires cause tree mortality, release nutrients (Kulmala et al., 2014) and create open space in the forest, which helps vegetation to grow from seeds (Venevsky et al., 2002; Moritz et al., 2012; Ramberg, 2020). Prescribed and reoccurring fires are needed to increase structural heterogeneity within a landscape and are pivotal for maintaining high biodiversity (Kuuluvainen, 2002; Ramberg, 2020). Mostly, total ecosystem recovery from severe forest fires is possible, but it will take a long time. Recovery of the forest floor mass could take several years, and for organic horizons, up to 20 years (Mäkipää et al., 2023). Fire may heat the soil to high temperatures and cause carbon and nutrient losses, soil physical alterations, stability of organic matter, and mortality of faunal and microbial communities (Mäkipää et al., 2023). Burning may also have a negative impact on carbon storage due to the losses of C and N in the ecosystem during the fire (Mäkipää et al., 2023; Mäkelä, 2015). Forest fires are a source of black carbon that is harmful to the health and accelerates the melting of snow and ice in the Arctic (Aalto and Venäläinen, 2021). In addition, forest fires may release pollutants, such as mercury (Hg), into the atmosphere, which may cause health problems (Turetsky et al., 2006). Fires cause greenhouse gas emissions (e.g. carbon dioxide CO_2) to be released into the atmosphere, which can further propagate climate change.

Forest fires are a result of interactions between climate, weather, fuel and humans (Flannigan et al., 2009; Lasslop et al., 2018). Warmer temperatures have a threefold link to wildfires due to increased evapotranspiration, lightning activity, and fire season (Flannigan et al., 2009). Climate change influences the spatial variations and the potential of extreme conditions of fire weather. Fire weather is defined as the weather variables (temperature, precipitation, humidity and wind) that influence fire behaviour, ignition and suppression (Flannigan et al., 2009).

The expected rate of temperature increase due to climate change in Fennoscandia is 2–3 times higher than the global average (Kaplan and New, 2006; Venäläinen et al., 2020). This expected acceleration increases the risk of forest fires, although an increase in precipitation might partially have the opposite effect (Mäkelä, 2015; Aakala et al., 2018; Kilpeläinen et al., 2010; Venäläinen et al., 2020). Across the boreal region, the burnt area and fire occurrences are projected to increase (Flannigan et al., 2009; de Groot et al., 2013) mainly due to temperature increase, but it is modulated by changes in precipitation, litter production, soil respiration and population density. Understanding the factors behind changes in forest fire activity is essential to ensure effective management of spreading fires (Jolly et al., 2015).

The main focus of previous studies has been the impact of varying meteorological conditions on fire risk (Flannigan et al., 2009; Ramberg, 2020; Mäkelä, 2015). Here, we use the land surface model JSBACH to study the fire season, number of fires and burnt area under changing climate. In this study, we investigate how and why projected climate change modulates the

forest fire risk in Fennoscandia. We present results from an analysis of climate change impacts on fire season, the number of fires and burnt area based on the JSBACH-SPITFIRE model simulations that were forced by downscaled and bias-corrected EURO-CORDEX data. The simulations were made under two climate change scenarios (RCP 4.5 and RCP 8.5) and three global climate driver models (CNRM-CM5, MIROC5 and CanESM2) from 1951 to 2100.

2 MATERIALS AND METHODS

2.1 Ecosystem model JSBACH

The JSBACH ecosystem model (Kaminski et al., 2013) was developed as the land surface component of the Earth System Models of the Max-Planck Institute for Meteorology (Reick et al., 2021; Mauritsen et al., 2019). The SPITFIRE (SPread and InTensity of FIRE) is a mechanistic global fire model (Thonicke et al., 2010) that has been implemented in the JSBACH ecosystem model (Lasslop et al., 2014). The forest fires in the JSBACH-SPITFIRE ecosystem model are disturbances that depend on weather conditions, fuel properties and population density.

The amount of fuel is estimated from the Yasso07 above-ground C-pools (Goll et al., 2015). It is simulated as a balance between litter produced by the vegetation and soil carbon decomposition, including combustion and consequent dead wood input from fire events. The fuel is divided into fuel classes according to reaction time to atmospheric conditions: 1 h, 10 h, 100 h and 1000 h fuel. The division represents different sizes, i.e. the different surface-area-to-volume ratios, of the fuel elements such as leaves, branches and trunks (Lasslop et al., 2014). The time required to reach the equilibrium moisture content under defined atmospheric conditions is longer with larger fuel elements due to a lower surface-area-to-volume ratio than for fine fuel elements. Grass (live fuel) is included in the 1 h fuel class. After a fire, the burnt carbon is subtracted from the C-pools and released in to the atmosphere as CO_2 and carbon from tree mortality is added to the C-pools (Thonicke et al., 2010).

The moisture content of the fuel is exponentially dependent on the Nesterov index (NI), and NI is weighted by the relative amounts of three fuel classes (1h – 100 h). The NI describes the drying power and depends on both temperature and precipitation. The NI (Onderka and Melicherčik, 2010) is a cumulative function of daily maximum and dew point temperature. The index is summed over days when the daily precipitation is less than 3 mm and the dew point temperature is above zero degrees (Thonicke et al., 2010; Running et al., 1987).

In JSBACH-SPITFIRE, the fire danger index (FDI) is the probability that an ignition event will cause a spreading fire. The FDI is one for completely dry fuel and zero for insufficient or wet fuel. The FDI is calculated from environmental dryness, temperature and the availability of fuel (Reick et al., 2021) as follows

$$FDI = \begin{cases} 1 - \frac{\text{fuel moisture}}{\text{moisture of extinction}}, & \frac{\text{fuel moisture}}{\text{moisture of extinction}} \leq 1 \\ 0, & \frac{\text{fuel moisture}}{\text{moisture of extinction}} > 1 \end{cases} \tag{1}$$

We used the FDI to estimate the number of days with high fire risk. An FDI > 0.8 indicates very high or extremely high fire risk (Thonicke et al., 2010). The fire season is the period when the FDI is above zero, and forest fires are possible. We defined the length of the fire season as the number of days between the first and last day when the FDI is greater than zero.

3

In the SPITFIRE, the fire may start from lightning ignition or a human act. The total ignition rate is the sum of lightning and human-caused ignitions. The expected number of human-caused ignition events depends on the population density and the propensity of people to cause ignition events (Thonicke et al., 2010), which reflect regional and cultural differences (Lasslop and Kloster, 2017). The number of human-caused ignition events is a non-linear function of population density. The ignition events increase with population density until it starts to decline due to landscape fragmentation, urbanisation and associated infrastructure changes (Thonicke et al., 2010). When there is fuel available, and the fuel is dry enough, the ignition will lead to a spreading fire. The number of fires per area is obtained by multiplying the number of total ignition events by the FDI. The burnt area is determined based on the number of fires, fire duration and the rate of spread (Rothermel, 1972), assuming an elliptical spread pattern (Carmody, 1992). The analysed burnt area is calculated for forested area. Overlapping fires were not accounted for, but such occurrences are very rare within the study area.

2.2   Regional simulations

Regional simulations were performed using the JSBACH-SPITFIRE ecosystem model over the period 1951–2100. The simulations were forced by downscaled and bias-corrected data from the EURO-CORDEX initiative (Jacob et al., 2014). We used data on the Eur-44 domain (Earth System Grid Federation Data Node), which was re-gridded to a regular 0.5° lat-lon grid, using nearest neighbour interpolation. The simulated model domain (Fig. 1 a) was limited to the land area within 55–71° N and 5–34° E.

The global models were forced under two Representative Concentration Pathway (RCP) scenarios: RCP 4.5 and RCP 8.5, with the number indicating radiative forcing values in Wm^{-2} in 2100 (van Vuuren et al., 2011). The RCP 4.5 scenario represents intermediate and RCP 8.5 high greenhouse gas emissions. While global mean surface temperature is likely to increase from 1.1°C to 2.6°C under RCP 4.5 and from 2.6°C to 4.8°C under RCP 8.5 by the end of the 21 century relative to 1986-2005 (IPCC, 2014), in Finland the multimodel annual mean temperature increases are 1.9, 3.3. and 5.6 C for RCPs 2.6, 4.5 and 8.5 respectively (Ruosteenoja et al., 2016). The RCPs share a common GHG pathway up to 2005 (the historical period) and deviate from there on (scenario period). The regional climate model RCA4 (Samuelsson et al., 2011) was used as a downscaling model for all three global climate driving models (CNRM-CM5, MIROC5 and CanESM2), and a distribution-based bias-correction method (SMHI-DBS45-EOBS12-1981-2010) was applied for all data sets that we used e.g. Yang et al. (2010). The daily bias-corrected data of precipitation and temperature for both RCP 4.5 and RCP 8.5 were used. In addition, daily data for relative humidity, wind speed and longwave and shortwave radiation were used.

A spin-up of the soil carbon pools was made before the actual simulation using driver data randomly generated from 1951–1980 and a prescribed CO_2 concentration (285 ppm). The JSBACH model was run with a timestep of 30 minutes, and values for the variables were output with a daily frequency. The land cover in the simulations represents the current land cover and was derived from the Finnish CORINE and the European CORINE (European Environment Agency, 2020) data. The ESA LandUse-CCI (European Space Agency, 2019) data was used for the area not covered by CORINE data. The land cover classes were translated into the 11 plant functional types that the JSBACH model uses. Land cover changes were not accounted for.

120   Soil properties were set according to Hagemann and Stacke (2015) so that the peat fraction of the land area was set according to the map by Xu et al. (2017), while the parameter values of Loamy Sand were assumed for the remaining land area.

    The human-caused ignition events were calculated from population density. The historical population density was based on data from the History Database of the Global Environment (Klein Goldewijk et al., 2017). The future scenario follows a middle-of-the-road shared socioeconomic pathway (SSP2) (Jones and O'Neill, 2016). The lightning ignition rate was obtained

125 from a climatology for Northern Europe compiled by the Finnish Meteorological Institute (Mäkelä et al., 2014) that was based on observations from lightning location sensors. The LIS/OTD 0.5 Degree High Resolution Monthly Climatology was used east of 32E (Cecil, 2016). The LIS/OTD climatology reports total flashes, but only about 20 % are cloud to ground flashes, which was taken into account. In addition, a latitude-dependent relation between total flashes and cloud-to-ground flashes was applied to correct the latitude bias in the LIS/OTD data (Pierce, 1970; Lasslop et al., 2014).

130   The simulations were initially set up for the study report Aalto and Venäläinen (2021) about current knowledge of the occurrence, monitoring, modelling and suppression of forest fires in Fennoscandia. Simulations were further improved for this study to match better the observed annual number of fires and burnt areas. Fire duration D_{fire} depends on population density P_{D} and fire danger index FDI (Eq. 1) as follows (Lasslop and Kloster, 2017)

$$D_{\text{fire}} = \begin{cases} \frac{241 \cdot 3}{1 + 240 \cdot e^{-11.06 \cdot FDI}}, P_{\text{D}} \leq 0.01 \\ \frac{241 \cdot (4 - \log(P_D)) \cdot 0.5}{1 + 240 \cdot e^{-11.06 \cdot FDI}}, 0.01 < P_{\text{D}} < 100 \\ \frac{241}{1 + 240 \cdot e^{-11.06 \cdot FDI}}, P_{\text{D}} \geq 100 \end{cases} \tag{2}$$

135 The default maximum fire duration (Eq. 2) was reduced from 720 min to 138 min to fit better the reported number of fires and burnt areas (Statistic system of Finnish rescue service database PRONTO, Pelastustoimen resurssi- ja onnettomuustilasto järjestelmä, PRONTO) in Finland. PRONTO data was available from 2011 to 2018, and wildfires, except fires in fields, grasslands, roadsides and landfills, were selected. The observations were compared to the simulated data for the period 1991–2020. For the models, the 30-year average is more reliable than the shorter seven-year PRONTO period, as the forcing data do not represent

140 the conditions in any given year. The simulated number of fires was in line with the observed values for Finland, which has a low population density. At high population densities, i.e. in urban areas, the simulations underestimated the number of fires (Fig. A1 a) and burnt areas (Fig. A1 b) compared to observations.

2.3   Model domain and data analysis

    The monthly or annual means for 9 daily simulated fire variables (FDI, number of fires, burnt area, CO_2 flux, gross primary

145 productivity, litter flux, soil respiration, fuel and fuel moisture) and 3 derived variables (start day, end day and number of very high and extremely high FDI days) are in dataset Kinnunen (2024). Distributions of fire-related variables were analysed and presented as maps. Additionally, in order to investigate the spatial differences in temporal dynamics in more detail, six example locations around the domain were chosen to be shown in a time series. The selected locations represented different vegetation zones: Location I in the Northern boreal, Location II and III in the Middle boreal, Location V in the Southern boreal, as well

as Location IV and Location VI in the Hemiboreal-Nemoral (Elmhagen et al., 2015). In the selected locations, the fractions of coniferous vegetation were at least 40 % (Fig. 1 a).
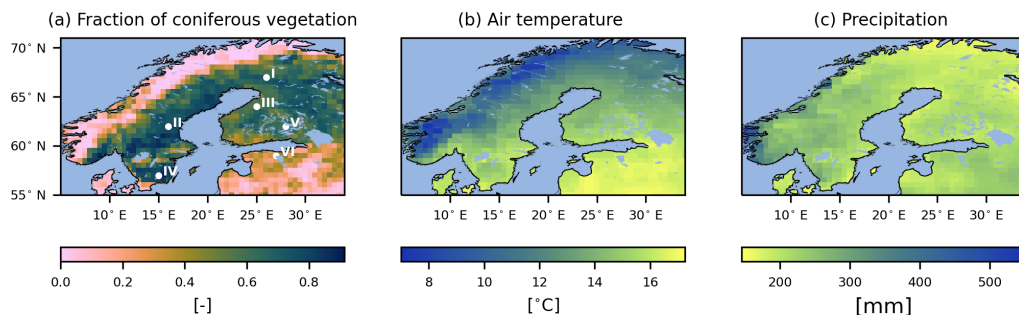
Figure 1. (a) The model domain: Fraction of coniferous vegetation and example locations. Location I is in northern Finland (67° N 26° E) 0.728, location II is in central Sweden (62° N 16° E) 0.832, Location III is in central Finland (64° N 25° E) 0.534, Location IV is in southern Sweden (57° N 15° E) 0.833, Location V is in southern Finland (62° N 28° E) 0.566 and Location VI is in Estonia (59° N 27° E) 0.401. (b) Average air temperature [°C] for June, July and August in the reference period 1981–2010 over all the climate projections. (c) Average precipitation [mm] for June, July and August during the reference period 1981–2010 over all all climate projections.

The reference period 1981–2010 values were calculated as an average of all climate projections. This choice was made because the RCPs and, therefore, climate models only started to deviate from 2006 onwards. In the summer months of June, July and August (JJA), the multi-model average temperature in the domain was 10 °C, increasing from northern to southern and western to eastern (Fig. 1 b). Multi-model average precipitation for summer months in the domain was 220 mm per year (Fig. 1 c).

The data analysis and plots were done with Python standard functions. The Mann-Kendall trend test ($p \leq 0.05$) was used to test for monotonic trends as implemented in the pyMannKendall package (Hussain and Mahmud, 2019). The colour scales were selected from the scientific colour maps (Crameri et al., 2020).

For every modeled grid point, multi year averages were calculated for the summer months (JJA) of FDI, air temperature, precipitation, fuel moisture and number of very high and extremely high FDI days. For ignition rates and the annual number of fires and the burnt area multi year averages were calculated. Changes in the variables were presented as the difference between averages of the period 2071–2100 and the reference period 1981–2010. We calculated the mean of the average changes over the domain in land grid points. The change in monthly climatologies (air temperature, precipitation and gross primary productivity) was calculated as a difference between periods 1981–2010 and 2017–2100 in six locations. The relative change was calculated as a ratio of the average of each period, 2071–2100 and 1981–2010 for litter flux, soil respiration and the amount of fuel.

The relative CO_2 flux change over time was calculated by comparing the 30-year moving average with the 1981–2010 mean value to smooth out the annual variations and show the overall trend. The time series were created to analyse the trend in the variables, such as the start and end dates of the fire season. The difference between the average start day and end day of the fire season was calculated to see whether the fire season changed more at the beginning or at the end of the season.

3 RESULTS

The largest increase in the summer months (JJA) temperature (ca. 4 °C – 7 °C) is observed under RCP 8.5 CanEMS2 from the period 1981–2010 to 2071–2100 (Fig. A2). The summer temperature increase is larger in the northern study locations, for example, Location I, than in the southern area, for example, Location IV (Fig. A3). The change in summer precipitation varied regionally (Fig. A4). The highest precipitation increase (ca. 40 %) is observed under RCP 8.5 CNRM-CM5. The change in monthly average precipitation from the period 1981–2010 to 2071–2100 varies significantly depending on the climate projection and the location (Fig. A5). The average gross primary productivity (GPP) during the summer months is greater during the 2071–2100 period than in the reference period 1981–2010 (Fig. A6).

The litter flux and soil respiration increase, and the amount of fuel decreases for the years 2071–2100 compared to the reference period 1981–2010 (shown for MIROC5 in Fig. A7). In many areas, projections suggest decreasing the amount of fuel available for fires because the increase in soil respiration compensates for the increase in litter flux.

Typically, the relative fuel moisture (Fig. A8) is projected to decrease due to an increase in the temperature (Fig. A2). This decrease in moisture leads to drier and more flammable fuel. The exception is under CNRM-CM5, when fuel moisture is expected to increase. Especially under RCP 4.5 CNRM-CM5, the fuel appears to be moister in the southern part of the simulated area. The CanESM2 global climate driver has the highest temperature increase and projects the greatest decrease in the relative fuel moisture.

3.1 Fire risk and season

The fire danger index (FDI) indicates the fire risk (Fig. 2) and increases with decreasing fuel moisture (Fig. A8). The FDI multi-model averaged over the whole domain land area is 0.2 ± 0.08 for the period 1981–2010 (Fig A9 a). Over that period, there are, on average days of 12 ± 6 very high or extremely high fire danger (FDI > 0.8) during the summer months (Fig A9 b). All simulations (except those driven by RCP 4.5 CNRM-CM5) forecast an increase in the probability of spreading fires in Fennoscandia in the summer months (JJA) from the period 1981–2010 to 2071–2100. The increase in the average FDI is from 0.05 ± 0.04 to 0.14 ± 0.03 (Fig. 2), and the increase in the number of very high or extremely high fire danger days is from (4 ± 3) days to (12 ± 3) days (Fig. A10) as the domain average by the end of the century.

According to the study locations, the results for the average changes and their standard deviations (std) of the start day, the end day, and the length of the fire season (see Fig. 1 a) are presented in Table B1. The start date change varies from (-6.8 $\pm$ 24.7) days to (-32.4 $\pm$ 31.6) days, and the end date from (2.3 $\pm$ 23.7) days to (33.2 $\pm$ 28.3) days. The lengthening of the fire season varies from (10.7 $\pm$ 34.1) days to (59.1 $\pm$ 39.0) days. As a day of the year, the start day of the fire season varies from

7
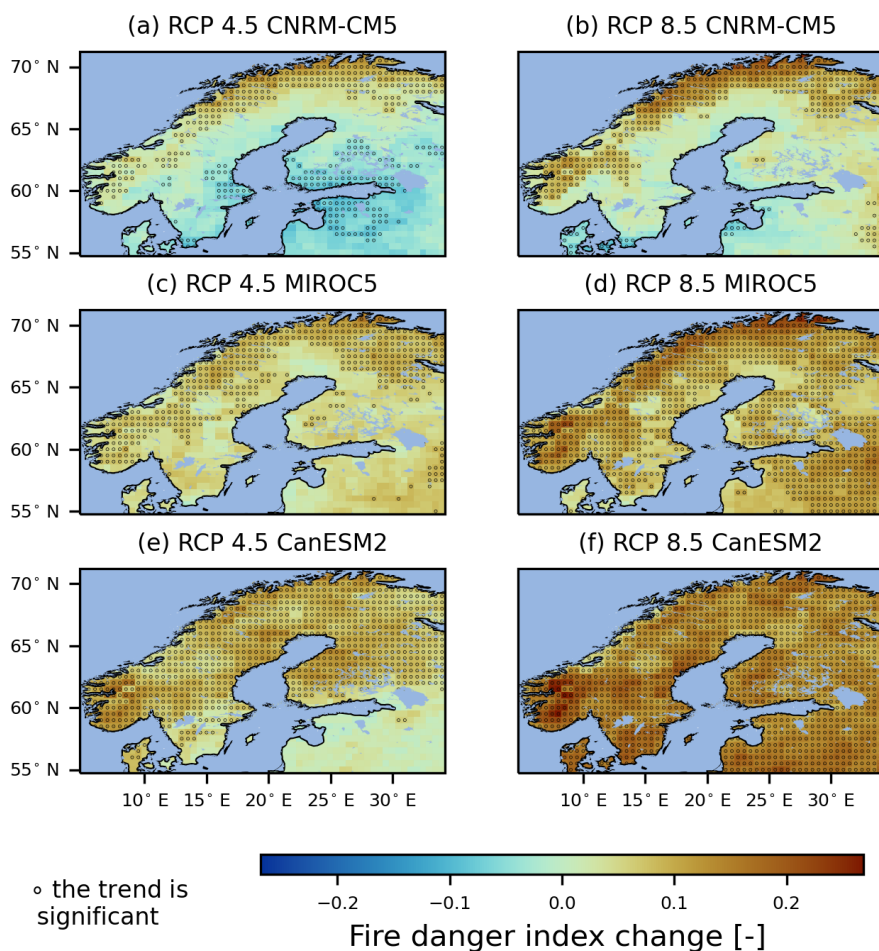
Figure 2. Relative changes in the fire danger index (unitless) for the summer months (JJA) average from the reference period 1981–2010 to 2071–2100 under two climate change forcing scenarios and three global driver models. Red indicates an increase, and blue indicates a decrease in the probability of spreading fire from ignition. The dots indicate a significant trend according to the Mann-Kendall test ($p \leq 0.05$).

88–211 and the end day from 197–326 in the study locations (Fig. 3). The fire season is assumed to extend by starting at the earliest at the end of March (Location IV) and ending at the latest in November (Location VI). The trends of fire season start and end dates are significant according to the Mann-Kendall trend test ($p \leq 0.05$), except for the start date under CNRM-CM5 at Locations II and III and for the end date at Location IV. In the southern part, the fire season is longer, and its lengthening is more extensive than in the northern part.

In the reference period 1981–2010, the length of the fire season is from (87 ± 36) days to (92 ± 34) days as, averaged over the model domain land area. The length of the fire season is projected to increase from (20 ± 7) days to (52 ± 12) days on average in

**Table 1.** Average number of fires in Finland and the change by the end of the century.

Source	Average 1981–2010 (std)	Average 2071–2100 (std)	Change (std)	% (std)
RCP 4.5 CNRM-CM5	1416 (487)	1320 (470)	-96 (616)	-7 (-4)
RCP 8.5 CNRM-CM5	1386 (488)	1569 (522)	183 (748)	13 (7)
RCP 4.5 MIROC5	1447 (510)	1807 (523)	360 (703)	25 (2)
RCP 8.5 MIROC5	1477 (611)	2273 (532)	797 (814)	54 (-13)
RCP 4.5 CanESM2	1253 (503)	1916 (627)	663 (891)	53 (25)
RCP 8.5 CanESM2	1268 (445)	2516 (695)	1248 (632)	98 (56)

the whole model domain land area (Fig. A11). The fire season is estimated to extend from (10±9) days to (23±11) days at the beginning of the fire season and from (10±10) days to (30±16) days at the end of the fire season. When the average change in the start date of the fire season is greater than the change in the end date, the fire season length increases more at the beginning than at the end of the season. For example, in Location I, the total lengthening of the fire season is 23 days under RCP 4.5 CNRM-CM5 and RCP 4.5 MIROC5, but the change is more considerable at the end of the season in the first case and at the beginning of the season in the second case (Table B1). The lengthening of the fire season is projected to primarily take place at the beginning of the season (max 71 % of grid points) under the CNRM-CM5 and MIROC5 global driver models and in at end of the season (max 79 % of grid points) under the CanESM2 global driver model (Fig. A12).

3.2 Number of fires and burnt area

The simulated human caused ignition rate depends on the population density and has a spatial variation in the range of (0–0.0012) $\text{km}^{-2}\text{yr}^{-1}$ (Fig. A13 a). The lightning caused ignition rate has a maximum value around 0.0002 $\text{km}^{-2}\text{yr}^{-1}$ (Fig. A13 b). Lightning ignition rate is, on average, 7 % of the total ignition rate. The average total ignition rate of 2071–2100 in the eastern part of the model domain decreases, and in the western part of the model domain, it increases compared to the reference period 1981–2010 due to the change in human ignition rate. The change in the total ignition rate is from -0.0005 $\text{km}^{-2}\text{yr}^{-1}$ to 0.0006 $\text{km}^{-2}\text{yr}^{-1}$ and average (-0.00003 ± 0.00011) $\text{km}^{-2}\text{yr}^{-1}$ (Fig. A13 c).

The number of fires during the reference period (Fig. A9 c) is (0.004 ± 0.003) $\text{km}^{-2}\text{yr}^{-1}$ as a multi-model average over the whole domain and increases, depending on the model, from (0.0006 ± 0.0007) $\text{km}^{-2}\text{yr}^{-1}$ to (0.003 ± 0.003) $\text{km}^{-2}\text{yr}^{-1}$ by the end of the century. However, especially in CNRM-CM5, there are regions of significant decrease by the end of the century (Fig. 4). In Finland, the change in the number of fires is from (-96 ± 616) fires per year to (1248 ± 631) fires per year, or (-7 ± 4) % to (98 ± 56) % (Table 1). The simulated values of the average number of fires in Finland from 1355 ± 509 to 1568 ± 556 match the values 1691 ± 799 observed in the PRONTO data (Table 2). The average number of fires per year is greater in the southern part than in the northern part of Finland, according to both the PRONTO data and the simulations (Fig. A14). The general pattern is the same, but the simulated values are more evenly distributed and do not increase as strongly with population density in cities.
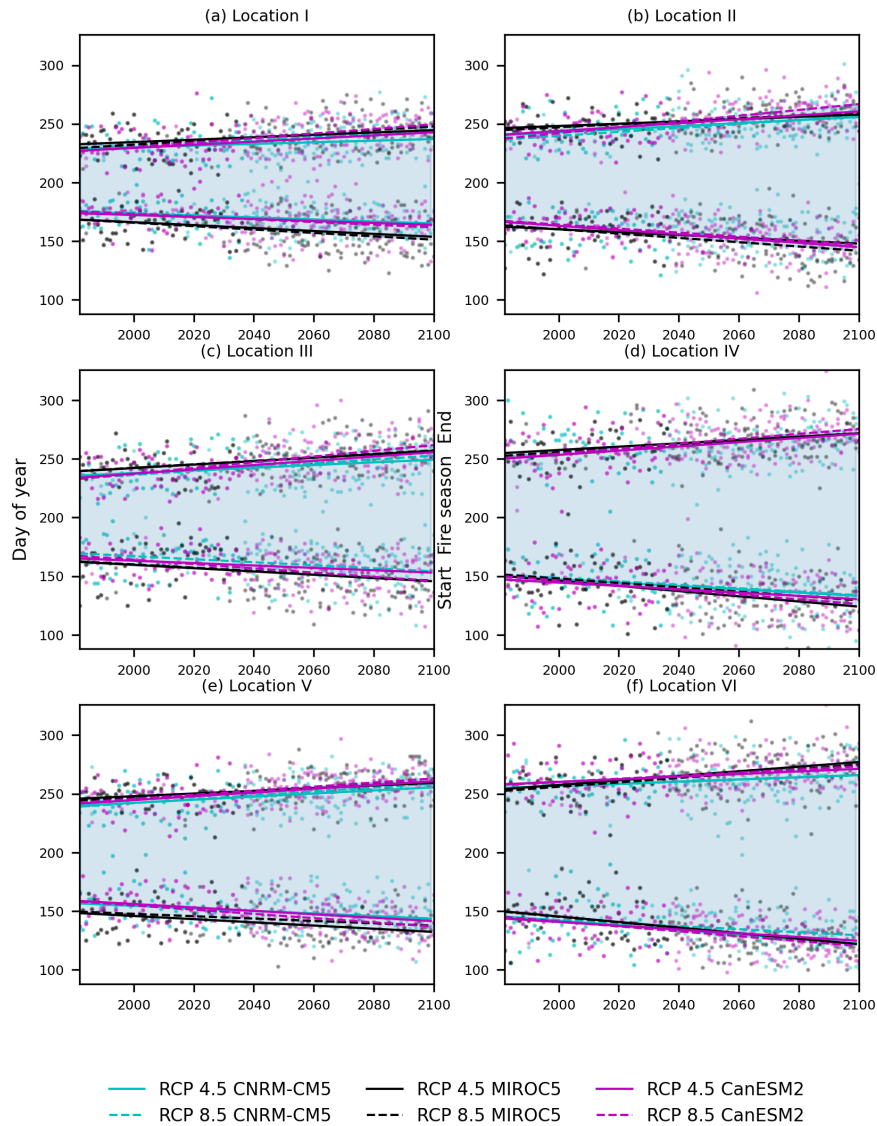
Figure 3. Future change in the fire season. Yearly values are dots, and the blue area between trend lines on the start and end dates is the fire season under two climate change forcing scenarios and three global driver models. Trends that are insignificant according to the Mann-Kendall trend test (p ≤ 0.05) are not shown, i.e. the start under CNRM-CM5 at Locations II and III and the end at Location IV. See locations in Fig. 1 a).

Table 2. The average number of fires in Finland during 2011–2018 from PRONTO data and 1991–2020 for simulations.

Source	Average	Std	Max	Min
PRONTO data	1691	799	3365	652
RCP 4.5 CNRM-CM5	1419	331	2362	909
RCP 8.5 CNRM-CM5	1414	372	2363	785
RCP 4.5 MIROC5	1534	448	2384	710
RCP 8.5 MIROC5	1568	556	3409	692
RCP 4.5 CanESM2	1355	509	2655	410
RCP 8.5 CanESM2	1419	436	2167	429

230   The multi-model average burnt area throughout the domain in the reference period is (0.02 ± 0.02) km^{2}yr^{-1} (FigA9). The increase in the average burnt area by the end of the century is from (0.004 ± 0.005) km^{2}yr^{-1} to (0.02 ± 0.02) km^{2}yr^{-1} depending on the model (Fig. 5). Overall, the changes in the burnt area vary a lot between the model simulations and spatially, even within a single simulation. The greatest increase of up to around 0.05 km^{2}yr^{-1}, takes place in the southern parts of the domain in RCP 8.5 in CanESM2, while the largest decrease of -0.02 km^{2}yr^{-1} is seen in the middle of the domain in RCP 4.5
235 in CNRM-CM5.

According to the simulations, the burnt area in Finland is estimated to change (-1.52 ± 4.59) km^2 to (5.66 ± 5.40) km^2 or from (-18.78 ± 24.1) % to (86.64 ± 41.57) % from the reference period to the end of the century (Table 3). This results in a net burnt area of ranging from (6.55 ± 4.27) km^2 to (12.49 ± 6.26) km^2 by the end of the century. The burnt area in the simulations ranged from 7.33 km^2 $\pm$ 3.77 km^2 to 10.73 km^2 $\pm$ 5.86 km^2 in Finland. Compared to the PRONTO data (5.84
240 km^2 $\pm$ 3.93 km^2), the simulations slightly overestimate the burnt area, but the dispersion interval covers the averages of the modeled values (Table 4).

Table 3. The average burnt areas in Finland and the change by the end of the century.

Source	Average 1981–2010 (std) [km^2]	Average 2071–2100 (std) [km^2]	Change (std) [km^2]	% (std)
RCP 4.5 CNRM-CM5	8.07 (4.27)	6.55 (3.24)	-1.52 (4.59)	-19 (-24)
RCP 8.5 CNRM-CM5	7.48 (4.27)	7.64 (4.02)	0.16 (6.00)	2 (-6)
RCP 4.5 MIROC5	9.48 (5.47)	10.51 (5.19)	1.03 (7.75)	11 (-5)
RCP 8.5 MIROC5	9.79 (6.26)	12.49 (5.20)	2.70 (7.86)	28 (-17)
RCP 4.5 CanESM2	6.66 (4.22)	10.45 (5.80)	3.79 (7.91)	57 (38)
RCP 8.5 CanESM2	6.54 (3.84)	12.20 (5.43)	5.66 (5.40)	87 (42)

The distribution of the average burnt area in 293 grid points located in Finland shows that the average annual burnt area per grid point is assumed to increase from the period 1981–2010 to 2071–2100 (Fig. A15). This increase is seen in all simulations except under RCP 4.5 CNRM-CM5. The amount of emitted CO_2 from fires follows the burnt area spatial patterns (Fig. 5).
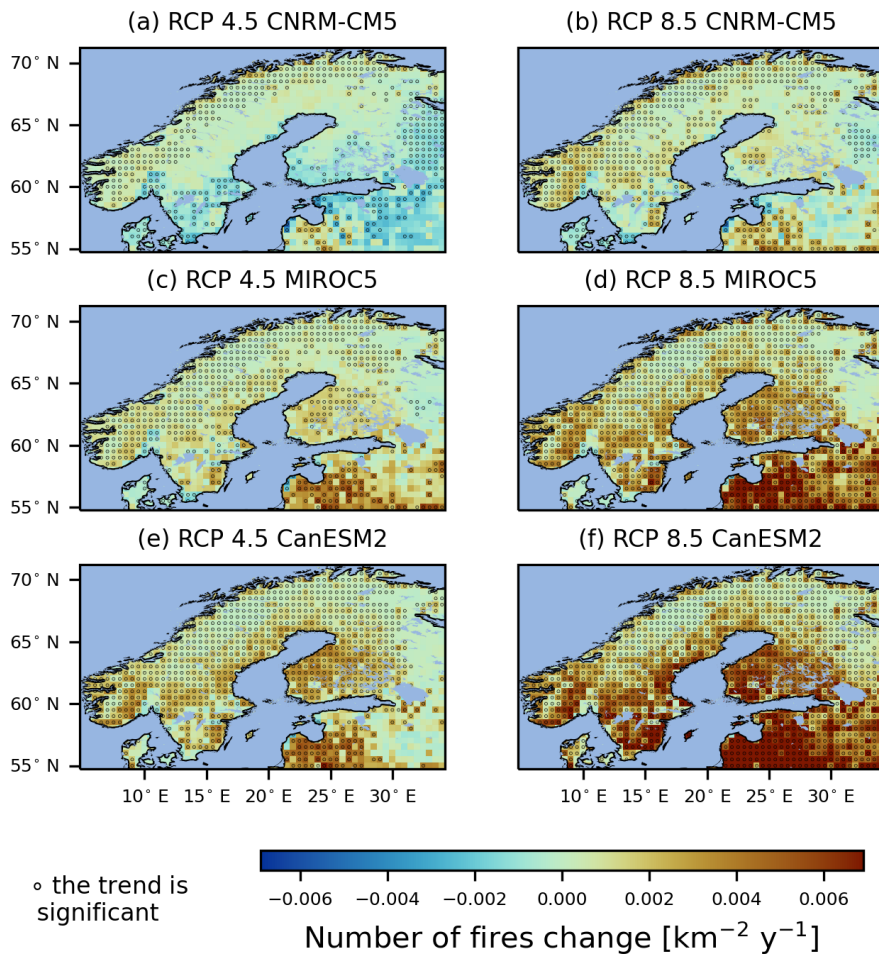
Figure 4. The average change in the annual number of fires $[\text{km}^{-2}\text{yr}^{-1}]$ from the reference period 1981–2010 to 2071–2100 under two climate change forcing scenarios and three global driver models. The red indicates more fires at the end of the century. The colour bar maximum is limited to show the most important patterns. The dots indicate a significant linear trend according to the Mann-Kendall test (p ≤ 0.05).

245   The change of CO_2 flux from 2010 to 2100 compared to the reference period (1981–2010) is highly non-linear, indicating either an increase or decrease in CO_2 emissions, depending on the climate driver and location (Fig. A16).

4 DISCUSSION

Our results indicate a lengthening of the fire season and an increase in the number of fires and the burnt area, even though the changes in magnitude and even the signs of the changes vary between different driving models and locations. In our

Table 4. The average burnt areas in Finland during 2011–2018 from PRONTO data and 1991–2020 for simulations.

Source	Average [km^2]	Std [km^2]	Max [km^2]	Min [km^2]
PRONTO data	5.84	3.93	14.09	1.18
RCP 4.5 CNRM-CM5	7.68	3.10	14.93	3.01
RCP 8.5 CNRM-CM5	7.80	3.95	17.83	2.82
RCP 4.5 MIROC5	9.94	4.77	21.74	3.48
RCP 8.5 MIROC5	10.73	5.86	29.3	3.70
RCP 4.5 CanESM2	7.53	4.60	19.27	0.92
RCP 8.5 CanESM2	7.33	3.77	19.10	1.02

250 simulations, temperature and precipitation changes are the leading cause of changes in forest fire occurrence in Fennoscandia and wind effects to the rate of spread. Veira et al. (2016) report that by the end of the century, there can be area-specific changes in forest fire activity due to interactions between climate conditions, population density and land use. Land use changes were not accounted for. This does not have much impact on the results as according to Zhou et al. (2021) forested area have been relatively constant showing changes of the most prominent land cover class of up to ±5 %. Regarding the future Hoffmann

255 et al. (2023) reported projected land cover changes of up to ±10 % in most of the Fennoscandia.

In our simulations, the slight overall decrease in the amount of fuel is a net effect of the increases both in soil respiration and litter flux. Our analyses suggest that in Fennoscandia, fuel availability is not the main limiting factor for fires. The increase in temperature reduces the moisture content of the fuel, making the fuel drier and more flammable. We observed that fuel moisture is the one of the main drivers of the increase in the simulated fire risk. According to Flannigan et al. (2009), the

260 critical elements of fire occurrence and spread are fuel properties, such as type, continuity, structure, heterogeneity, moisture and volume. The fuel load depends on both the accumulation and decomposition of organic matter, which are affected by climate factors (Kilpeläinen et al., 2010). Moreover, the active management of fuel affects fires (North et al., 2012).

According to our study, the increase in the fire danger index indicates generally a higher probability of spreading fires at the end of the century. Nevertheless, under CNRM-CM5, we observed decreasing fire risk in the southern parts of the domain. In

265 Finland, Lehtonen et al. (2014) project fire risk to increase by (10–40) % by the end of the century, depending on the GHG scenario. Southern Sweden is projected to have a higher fire risk and northern Sweden to have a lower fire risk than today (Yang et al., 2015; Ramberg, 2020), which is contrary to our results that show an increasing gradient from south to north.

Our simulations indicate an increase from (4 ± 3) days to (12 ± 3) days days in the number of days of high or extremely high fire danger. Mäkelä (2015) concludes that forest fire danger varies considerably from year to year, and the increase in fire

270 danger days is (7–10) days at the end of the century in Finland. The realised change in the number of fires depends on many factors, but the potential for fires will increase due to changing climatological conditions (Mäkelä, 2015).

In our study, the projected increase in the average length of the fire season is from (20 ± 7) days to (52 ± 12) days. This increase is in line with Veira et al. (2016), who argue that the temperate and boreal fire seasons will become, on average, prolonged by (1–3) months for RCP 8.5 and with Flannigan et al. (2013), who speculate an increase of more than 20 days per
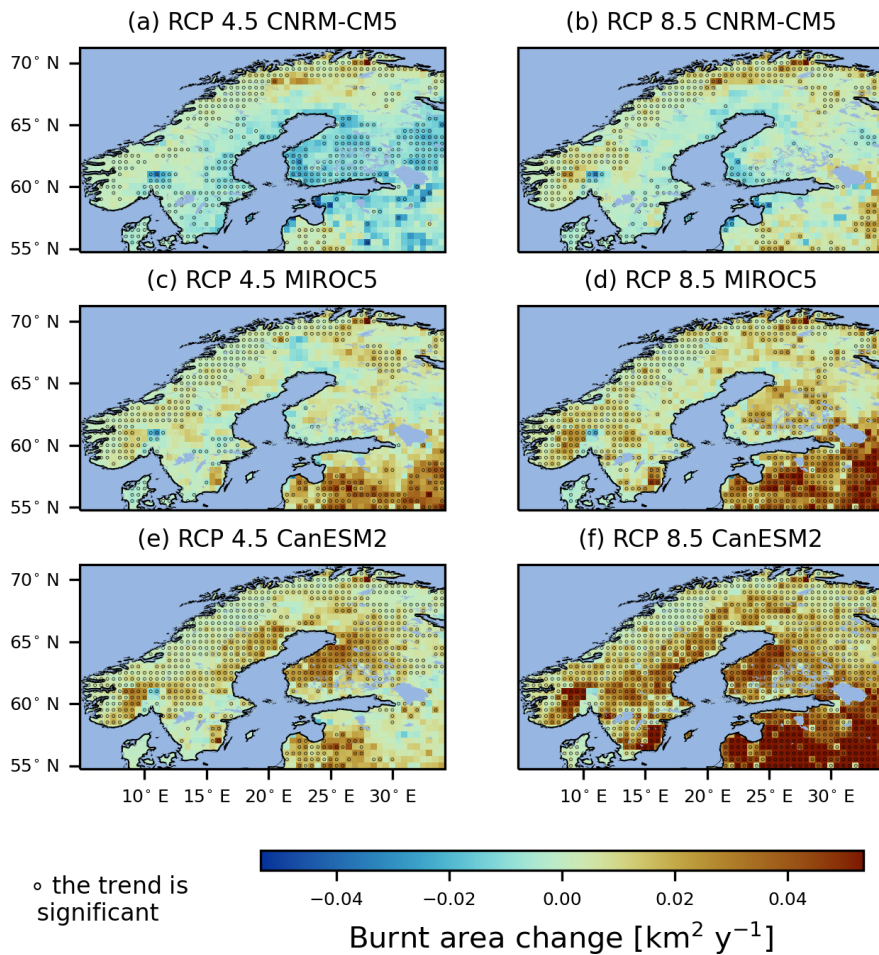
Figure 5. Change in the annual average burnt area $[\mathrm{km}^2\mathrm{y}^{-1}]$ from reference period 1981–2010 to 2071–2100 under two climate change forcing scenarios and three global driver models. Red indicates an increase in burnt area. The colour bar maximum is limited to show the most important patterns. The dots indicate a significant linear trend according to the Mann-Kendall test (p ≤ 0.05).

275 year in the length of the fire season for northern high latitudes. One reason for a longer fire season may be the shortened snow season, especially in southern Finland (Kilpeläinen et al., 2010). The impact of snow cover is not explicitly considered in our simulation. According to our simulations, the lengthening of the fire season is projected to happen typically at the beginning of the season due to warmer and drier weather. In a warming world, fire seasons should continue to lengthen in temperate and boreal regions (Flannigan et al., 2009).

280   In our simulations, the probability of lightning was prescribed with a daily climatology that does not include year-to-year variation. The number of days with thunderstorms and the average annual observed cloud-to-ground flash density do not show clear trends in Finland from 1887 to 2018 (Laurila and Mäkelä, 2019). However, Tuomi and Mäkelä (2008) observed large

spatial and annual variations in flash density over the 1998–2007 period. The risk of lightning-ignited fires may vary from a 62% decrease to a 38% increase under RCP 6.0 in the polar regions from the 2010s to the 2090s, according to one study Pérez-Invernón et al. (2023). Due to rising atmospheric instability, in the RCP4.5 and RCP8.5 scenarios, all model members predict relative changes in lightning frequency between 5% and 40% in Northern Europe until 2100 (Rädler et al., 2019). These variations in lightning frequency should be taken into account even though their contribution to the total ignition rate is, on average, only 7 %. Because in Fennoscandia, fires are caused mainly by humans (Mäkelä, 2015; Kilpeläinen et al., 2010) and the ignition rate in simulations is non-linearly dependent on population density, the impact of human ignition should also be further studied with different population density scenarios. Our study demonstrates the potential impacts of climate change to the fire season, number of fires and burnt area even though JSBACH do not include all relevant aspects of human-nature interaction such as active fire suppression, local landscape fragmentation, land use (e.g. roads) and lakes. Nevertheless, the fire duration limitation serves as a surrogate for fire suppression.

Our simulated annual number of fires in Finland is estimated to be in the range of 1355 ± 509 to 1568 ± 556 between 1991 and 2020, which is lower than the statistical (Finnish rescue service database PRONTO) value of 1691 ± 799. In the SPITFIRE model, the number of fires is constrained at high population density values, and the statistical value is determined based on emergency reports, encompassing all minor fires. We concluded that the yearly mean simulated burnt area in Finland is from $(7.33 \pm 3.77)\ \mathrm{km}^2$ to $(10.73 \pm 5.86)\ \mathrm{km}^2$ for the period 1991–2020. The observed burnt area through 2011–2018 is lower $(5.84 \pm 3.93)\ \mathrm{km}^2$ due to effective fire detection, management and extinguishing in Finland. As an average over a longer period and broader area, the values should be consistent with the statistical values, even though the simulations are based on scenario data and do not represent the weather conditions of an actual year. Lehtonen et al. (2016) point out that all over Finland, the fire risk, the number of large fires (>10 ha) and the burnt area are increasing, although due to the current small fire area, one large fire affects the statistics. Larger and more intense fires are expected in a future warmer world (Flannigan et al., 2013).

Previous studies show that the SPITFIRE captures the response of a burnt area to precipitation well (Lasslop et al., 2018). There is considerable variation in the fire occurrence between different times and regions due to changes in the natural and anthropogenic causes impacting the fires (Aakala et al., 2018; Flannigan et al., 2009).

The calibration of the SPITFIRE model may be further improved by the use of observational data sets covering the whole domain and subsequent tuning of model parameters.

Changes in human activities and weather conditions cause uncertainty regarding fire risk prediction (Aalto and Venäläinen, 2021).

5 Conclusions

In this study, we have studied the projected changes in fire season, number of fires and burnt area over Fennoscandia from the reference period (1981–2010) to the end of the century (2071–2100) using ecosystem model simulations from 1951 to 2100.

The simulations suggest increased fire danger due to drier and, thus more flammable fuels towards the end of the century. Increasing soil litter decomposition compensates for the increase in litter input, and less fuel may be available for fires. However, the decrease in fuel is not meaningful enough to limit the occurrence of spreading fires.

Our simulations suggest that the fire season is extended, and the lengthening of fire seasons happens primarily at the beginning of the season. Nevertheless, the spatio-temporal variations in the fire variables depending on global climate driver models (CanESM2, MIROC5 and CNRM-CM5) and regions imply uncertainty in the degree of change. The highest change in temperature leads to an increased fire risk and causes more fires and a larger burnt area, whereas the largest increase in precipitation reduces the fire risk, the number of fires and the burnt area. Moreover, because human activity is the leading cause of fire ignition, our study pinpoints the need for the use of reliable human activity data in addition to improved climate scenario data.

Appendix A: Figures

Appendix B: Tables

Author contributions. OK prepared the manuscript with contributions from all co-authors. LB is responsible for the JSBACH ecosystem model simulations. OK performed the data analysis and produced the graphics and tables with contributions from co-authors. JA and TA have contributed to the design of the study. TM has coordinated the study.

References

335   Aakala, T., Pasanen, L., Helama, S., Vakkari, V., Drobyshev, I., Seppä, H., Kuuluvainen, T., Stivrins, N., Wallenius, T., Vasander, H., and Holmström, L.: Multiscale variation in drought controlled historical forest fire activity in the boreal forests of eastern Fennoscandia, Ecological Monographs, 88, 74–91, https://doi.org/https://doi.org/10.1002/ecm.1276, 2018.

Aalto, J. and Venäläinen, A.: Climate change and forest management affect forest fire risk in Fennoscandia, Finnish Meteorological Institute, Reports 2021:3, 2021.

340   Carmody, C.: Development and Structure of the Canadian Forest Fire Behaviour Predictions Systems, Forestry Canada Fire Danger Group, Scientific Sustainable Development Directory, Ottawa, Ont. Inf. Rep. ST-X-3, Ministery of Supply and Service Canada, 1992.

Cecil, D. J.: LIS/OTD 0.5 Degree High Resolution Monthly Climatology (HRMC). [2.3.2015] Dataset available online from the NASA Global Hydrology Resource Center DAAC, Huntsville, Alabama, U.S.A. https://ghrc.nsstc.nasa.gov/hydro/details/lohrmc NASA, Global Hydrology Resource Center, https://doi.org/http://dx.doi.org/10.5067/LIS/LIS-OTD/DATA303, 2016.

345   Crameri, F., Shephard, G., and Heron, P.: The misuse of colour in science communication., Nat Commun 11, 5444, https://doi.org/10.1038/s41467-020-19160-7, 2020.

de Groot, W. J., Flannigan, M. D., and Cantin, A. S.: Climate change impacts on future boreal fire regimes, Forest Ecology and Management, 294, 35–44, https://doi.org/https://doi.org/10.1016/j.foreco.2012.09.027, the Mega-fire reality, 2013.

Descals, A., Gaveau, D. L. A., Verger, A., Sheil, D., Naito, D., and Peñuelas, J.: Unprecedented fire activity above the Arctic Circle linked to
350   rising temperatures, Science, 378, 532–537, https://doi.org/10.1126/science.abn9768, 2022.

Earth System Grid Federation Data Node: Cordex Dataset, https://esgf-data.dkrz.de/search/cordex-dkrz/, accessed: 27 Feb 2020.

Elmhagen, B., Kindberg, J., and Hellström, P.: A boreal invasion in response to climate change? Range shifts and community effects in the borderland between forest and tundra., AMBIO 44 (Suppl 1), 39–50, https://doi.org/10.1007/s13280-014-0606-8, 2015.

Engelmark, O.: Boreal forest disturbances, in: Ecosystems of disturbed ground, edited by Walker, L. R., chap. 6, pp. 161–186, Elsevier, 1999.
355   European Environment Agency: Corine Land Cover (CLC) 2012, Version 2020_20u1, (accessed 2020, Jun 12), https://land.copernicus.eu/pan-european/corine-land-cover/clc-2012, 2020.

European Space Agency: Land cover classification gridded maps from 1992 to present derived from satellite observations, Copernicus Climate Data Store, (accessed 2020, Mar 30), https://cds.climate.copernicus.eu/cdsapp#!/dataset/satellite-land-cover, 2019.

Flannigan, M., Krawchuk, M., Wotton, M., and Johnston, L.: Implications of changing climate for global wildland fire, International Journal
360   of Wildland Fire, 18, 483–507, https://doi.org/10.1071/WF08187, 2009.

Flannigan, M., Cantin, M., Groot, A., Wotton, W., Newbery, M., and Johnston, L.: Global wildland fire season severity in the 21st century, Forest Ecology and Management, 294, 64–71, https://doi.org/10.1016/j.foreco.2012.10.022, 2013.

Goll, D. S., Brovkin, V., Liski, J., Raddatz, T., Thum, T., and Todd-Brown, K. E. O.: Strong dependence of CO_2 emissions from anthropogenic land cover change on initial land cover and soil carbon parametrization, Global Biogeochemical Cycles, 29, 1511–1523,
365   https://doi.org/https://doi.org/10.1002/2014GB004988, 2015.

Gromtsev, A.: Natural Disturbance Dynamics in the Boreal Forests of European Russia: a Review, Silva Fennica, 36, https://doi.org/10.14214/sf.549, 2002.

Hagemann, S. and Stacke, T.: Impact of the soil hydrology scheme on simulated soil moisture memory, Climate Dynamics, 44, 1731–1750, https://doi.org/10.1007/s00382-014-2221-6, 2015.

370   Hantson, S., Lasslop, G., Kloster, S., and Chuvieco, E.: Anthropogenic effects on global mean fire size, International Journal of Wildland Fire, 24, 589–596, https://doi.org/10.1071/WF14208, 2015.

Hoffmann, P., Reinhart, V., Rechid, D., de Noblet-Ducoudré, N., Davin, E. L., Asmus, C., Bechtel, B., Böhner, J., Katragkou, E., and Luyssaert, S.: High-resolution land use and land cover dataset for regional climate modelling: historical and future changes in Europe, Earth Syst. Sci. Data, 15, 3819–3852, https://doi.org/https://doi.org/10.5194/essd-15-3819-2023, 2023.

375   Hussain, M. and Mahmud, I.: pyMannKendall: a python package for non parametric Mann Kendall family of trend tests., Journal of Open Source Software, 4, 1556, https://doi.org/10.21105/joss.01556, 2019.

IPCC: Climate Change 2014: Synthesis Report. Contribution of Working Groups I, II and III to the Fifth Assessment Report of the Intergovernmental Panel on Climate Change, [Core Writing Team, R.K. Pachauri and L.A. Meyer (eds.)], 2014.

Jacob, D., Petersen, J., Eggert, B., Alias, A., Christensen, O., Bouwer, L., Braun, A., Colette, A., Déqué, M., Georgievski, G., Georgopoulou,
380   E., Gobiet, A., Menut, L., Nikulin, G., Haensler, A., Hempelmann, N., Jones, C., Keuler, K., Kovats, S., Kröner, N., Kotlarski, S., Kriegsmann, A., Martin, E., van Meijgaard, E., Moseley, C., Pfeifer, S., Preuschmann, S., Radermacher, C., Radtke, K., Rechid, D., Rounsevell, M., Samuelsson, P., Somot, S., Soussana, J.-F., Teichmann, C., Valentini, R., Vautard, R., Weber, B., and Yiou, P.: EURO-CORDEX: new high-resolution climate change projections for European impact research., Regional environmental change 14: 563–578., 2014.

Jolly, W., Cochrane, M., and Freeborn, P.: Climate-induced variations in global wildfire danger from 1979 to 2013., Nat Commun 6, 7537,
385   https://doi.org/10.1038/ncomms8537, 2015.

Jones, B. and O'Neill, B.: Global One-Eighth Degree Population Base Year and Projection Grids Based on the Shared Socioeconomic Pathways, Revision 01. Palisades, NY: NASA Socioeconomic Data and Applications Center (SEDAC)., https://doi.org/https://doi.org/10.7927/m30p-j498, accessed May 18 2020, 2016.

Kaminski, T., Knorr, W., Schürmann, G., Scholze, M., Rayner, P. J., Zaehle, S., Blessing, S., Dorigo, W., Gayler, V., Giering, R., Gobron, N.,
390   Grant, J. P., Heimann, M., Hooker-Stroud, A., Houweling, S., Kato, T., Kattge, J., Kelley, D., Kemp, S., Koffi, E. N., Köstler, C., Mathieu, P.-P., Pinty, B., Reick, C. H., Rödenbeck, C., Schnur, R., Scipal, K., Sebald, C., Stacke, T., van Scheltinga, A. T., Vossbeck, M., Widmann, H., and Ziehn, T.: The BETHY/JSBACH Carbon Cycle Data Assimilation System: experiences and challenges, Journal of Geophysical Research: Biogeosciences, 118, 1414–1426, https://doi.org/https://doi.org/10.1002/jgrg.20118, 2013.

Kaplan, J. and New, M.: Arctic climate change with a 2 °C global warming: Timing, climate patterns and vegetation change., Climatic
395   Change 79, 213–241, https://doi.org/10.1007/s10584-006-9113-7, 2006.

Kilpeläinen, A., Kellomäki, S., Strandman, H., and Venäläinen, A.: Climate change impacts on forest fire potential in boreal conditions in Finland, Climatic Change, 103, 383–398, https://doi.org/10.1007/s10584-009-9788-7, 2010.

Kinnunen, O.: Data for manuskript "Projected changes in forest fire season, number of fires and burnt area in Fennoscandia by the 2100" by Kinnunen etal, Finnish Meteorological Institute, https://doi.org/10.57707/FMI-B2SHARE.07695381224049C78BD35198D27AAA25,
400   version 1 [dataset], 2024.

Klein Goldewijk, K., Beusen, A., Doelman, J., and Stehfest, E.: Anthropogenic land use estimates for the Holocene – HYDE 3.2, Earth Syst. Sci. Data, 9, 927–953, https://doi.org/https://doi.org/10.5194/essd-9-927-2017, 2017.

Kulmala, L., Aaltonen, H., Berninger, F., Kieloaho, A.-J., Levula, J., Bäck, J., Hari, P., Kolari, P., Korhonen, J. F., Kulmala, M., Nikinmaa, E., Pihlatie, M., Vesala, T., and Pumpanen, J.: Changes in biogeochemistry and carbon fluxes in a boreal forest after the clear-cutting and
405   partial burning of slash, Agricultural and Forest Meteorology, 188, 33–44, https://doi.org/https://doi.org/10.1016/j.agrformet.2013.12.003, 2014.

Kuuluvainen, T.: Natural Variability of Forests as a Reference for Restoring and Managing Biological Diversity in Boreal Fennoscandia, Silva Fennica, 36, https://doi.org/10.14214/sf.552, 2002.

Larjavaara, M., Kuuluvainen, T., and Rita, H.: Spatial distribution of lightning-ignited forest fires in Finland, Forest ecology and management, 208, 177–188, 2005a.

Larjavaara, M., Pennanen, J., and Tuomi, T.: Lightning that ignites forest fires in Finland, Agricultural and Forest Meteorology, 132, 171–180, https://doi.org/https://doi.org/10.1016/j.agrformet.2005.07.005, 2005b.

Lasslop, G. and Kloster, S.: Human impact on wildfires varies between regions and with vegetation productivity, Environmental Research Letters, 12, 115 011, https://doi.org/10.1088/1748-9326/aa8c82, 2017.

Lasslop, G., Thonicke, K., and Kloster, S.: SPITFIRE within the MPI Earth system model: Model development and evaluation, Journal of Advances in Modeling Earth Systems, 6, 740–755, https://doi.org/https://doi.org/10.1002/2013MS000284, 2014.

Lasslop, G., Moeller, T., D'Onofrio, D., Hantson, S., and Kloster, S.: Tropical climate–vegetation–fire relationships: multivariate evaluation of the land surface model JSBACH, Biogeosciences, 15, 5969–5989, https://doi.org/10.5194/bg-15-5969-2018, 2018.

Laurila, T. K. and Mäkelä, A.: Thunderstorm observations in Finland – historical observations since 1887, FMI's Climate Bulletin: Research Letters, 1(2), 4, https://doi.org/10.35614/ISSN-2341-6408-IK-2019-13-RL, 2019.

Lehtonen, I., Ruosteenoja, K., Venäläinen, A., and Gregow, H.: The projected 21st century forest-fire risk in Finland under different greenhouse gas scenarios, Boreal Environment Research, 19, 127–139, 2014.

Lehtonen, I., Venäläinen, A., Kämäräinen, M., Peltola, H., and Gregow, H.: Risk of large-scale fires in boreal forests of Finland under changing climate, Natural Hazards and Earth System Sciences, 16, 239–253, https://doi.org/10.5194/nhess-16-239-2016, 2016.

Mauritsen, T., Bader, J., Becker, T., Behrens, J., Bittner, M., Brokopf, R., Brovkin, V., Claussen, M., Crueger, T., Esch, M., Fast, I., Fiedler, S., Fläschner, D., Gayler, V., Giorgetta, M., Goll, D. S., Haak, H., Hagemann, S., Hedemann, C., Hohenegger, C., Ilyina, T., Jahns, T., Jimenéz-de-la Cuesta, D., Jungclaus, J., Kleinen, T., Kloster, S., Kracher, D., Kinne, S., Kleberg, D., Lasslop, G., Kornblueh, L., Marotzke, J., Matei, D., Meraner, K., Mikolajewicz, U., Modali, K., Möbis, B., Müller, W. A., Nabel, J. E. M. S., Nam, C. C. W., Notz, D., Nyawira, S.-S., Paulsen, H., Peters, K., Pincus, R., Pohlmann, H., Pongratz, J., Popp, M., Raddatz, T. J., Rast, S., Redler, R., Reick, C. H., Rohrschneider, T., Schemann, V., Schmidt, H., Schnur, R., Schulzweida, U., Six, K. D., Stein, L., Stemmler, I., Stevens, B., von Storch, J.-S., Tian, F., Voigt, A., Vrese, P., Wieners, K.-H., Wilkenskjeld, S., Winkler, A., and Roeckner, E.: Developments in the MPI-M Earth System Model version 1.2 (MPI-ESM1.2) and Its Response to Increasing CO2, Journal of Advances in Modeling Earth Systems, 11, 998–1038, https://doi.org/https://doi.org/10.1029/2018MS001400, 2019.

Moritz, M. A., Parisien, M.-A., Batllori, E., Krawchuk, M. A., Van Dorn, J., Ganz, D. J., and Hayhoe, K.: Climate change and disruptions to global fire activity, Ecosphere, 3, art49, https://doi.org/https://doi.org/10.1890/ES11-00345.1, 2012.

Mäkelä, A., Enno, S.-E., and Haapalainen, J.: Nordic Lightning Information System: Thunderstorm climate of Northern Europe for the period 2002–2011, Atmospheric Research, 139, 46–61, https://doi.org/https://doi.org/10.1016/j.atmosres.2014.01.008, 2014.

Mäkelä, H.: Estimates of past and future forest fire danger in Finland from a climatological viewpoint, Finnish Meteorological Institute Contributions 112 - URN:ISSN:0782-6117, http://hdl.handle.net/10138/153233, 2015.

Mäkipää, R., Abramoff, R., Adamczyk, B., Baldy, V., Biryol, C., Bosela, M., Casals, P., Yuste, J. C., Dondini, M., Filipek, S., et al.: How does management affect soil C sequestration and greenhouse gas fluxes in boreal and temperate forests?: A review, Forest Ecology and Management, 2023.

North, M., Collins, B., and Stephens, S.: Using Fire to Increase the Scale, Benefits, and Future Maintenance of Fuels Treatments, Journal of Forestry, 110, 392–401, https://doi.org/10.5849/jof.12-021, 2012.

445   Onderka, M. and Meličerčik, I.: Fire-prone areas delineated from a combination of the Nesterov Fire-risk Rating Index with multispectral satellite data., Appl Geomat 2, 1–7, https://doi.org/10.1007/s12518-009-0014-0, 2010.

Pierce, E.: Latitudinal Variation of Lightning Parameters, Journal of Applied Meteorology, 9, 194–195, 1970.

Pérez-Invernón, F., Gordillo-Vázquez, F., Huntrieser, H., and Jöckel, P.: Variation of lightning-ignited wildfire patterns under climate change., Nature Communications, 14, https://doi.org/https://doi.org/10.1038/s41467-023-36500-5, 2023.

450   Ramberg, E.: The role of fire in the boreal forests of Fennoscandia: Past, present and future. Introductory Research Essay, Department of Ecology, Swedish University of Agricultural Sciences, https://res.slu.se/id/publ/104591, 2020.

Ramberg, E., Strengbom, J., and Granath, G.: Coordination through databases can improve prescribed burning as a conservation tool to promote forest biodiversity., Ambio, doi:10.1007/s13280-017-0987-6, 2018.

Reick, C. H., Gayler, V., Goll, D., Hagemann, S., Heidkamp, M., Nabel, J., Raddatz, T., Roeckner, E., Schnur, R., and Wilkenskjeld, S.:

455   JSBACH 3 - The land component of the MPI Earth System Model: Documentation of version 3.2., Berichte zur Erdsystemforschung, doi:10.17617/2.3279802, 2021.

Rothermel, R.: A mathematical model for predicting fire spread in wildland fuels., Res. Pap. INT-115. Ogden, UT: U.S. Department of Agriculture, Forest Service, Intermountain Forest and Range Experiment Station. 40 pp., 1972.

Running, S. W., Nemani, R. R., and Hungerford, R. D.: Extrapolation of synoptic meteorological data in mountainous terrain and its use for

460   simulating forest evapotranspiration and photosynthesis, Canadian Journal of Forest Research, 17, 472–483, https://doi.org/10.1139/x87-081, 1987.

Ruosteenoja, K., Jylhä, K., and Kämäräinen, M.: Climate projections for Finland under the RCP forcing scenarios., Geophysica, 51, 2016.

Rädler, A., Groenemeijer, P., Faust, E., Sausen, R., and Púčik, T.: Frequency of severe thunderstorms across Europe expected to increase in the 21st century due to rising instability., npj Climate and Atmospheric Science 2, 30, https://doi.org/https://doi.org/10.1038/s41612-019-

465   0083-7, 2019.

Samuelsson, P., Jones, C. G., Willén, U., Ullerstig, A., Gollvik, S., Hansson, U., Jansson, E., Kjellström, C., Nikulin, G., and Wyser, K.: The Rossby Centre Regional Climate model RCA3: model description and performance, Tellus A: Dynamic Meteorology and Oceanography, 63, 4–23, https://doi.org/10.1111/j.1600-0870.2010.00478.x, 2011.

Thonicke, K., Spessa, A., Prentice, I., Harrison, S., Dong, L., and Carmona-Moreno, C.: The influence of vegetation, fire spread and

470   fire behaviour on biomass burning and trace gas emissions: Results from a process-based model, Biogeosciences Discussions, 7, https://doi.org/10.5194/bgd-7-697-2010, 2010.

Tolonen, K. and Pitkänen, A.: Kulojen toistuvuus ja merkitys jääkauden jälkeisenä aikana Suomessa, 2004.

Tuomi, T. and Mäkelä, A.: Thunderstorm Climate of Finland 1998-2007, Geophysica, 44, 2008.

Turetsky, M. R., Harden, J. W., Friedli, H. R., Flannigan, M., Payne, N., Crock, J., and Radke, L.: Wildfires threaten mercury stocks in

475   northern soils, Geophysical Research Letters, 33, https://doi.org/https://doi.org/10.1029/2005GL025595, 2006.

Vajda, A., Venäläinen, A., Suomi, I., Junila, P., and Mäkelä, H.: Assessment of forest fire danger in a boreal forest environment: Description and evaluation of the operational system applied in Finland, Meteorological Applications, 21, https://doi.org/10.1002/met.1425, 2014.

van Vuuren, D., Edmonds, J., Kainuma, M., Riahi, K., Thomson, A., Hibbard, K., Hurtt, G., Kram, T., Krey, V., Lamarque, J., Masui, T., Meinshausen, M., Nakicenovic, N., Smith, S., and Rose, S.: The representative concentration pathways: an overview, Climatic Change

480   109:5–31, https://doi.org/10.1007/s10584-011-0148-z, 2011.

Veira, A., Lasslop, G., and Kloster, S.: Wildfires in a warmer climate: Emission fluxes, emission heights, and black carbon concentrations in 2090–2099, Journal of Geophysical Research: Atmospheres, 121, 3195–3223, https://doi.org/https://doi.org/10.1002/2015JD024142, 2016.

Venevsky, S., Thonicke, K., Sitch, S., and Cramer, W.: Simulating fire regimes in human-dominated ecosystems: Iberian Peninsula case study, Global Change Biology, 8, 984–998, https://doi.org/https://doi.org/10.1046/j.1365-2486.2002.00528.x, 2002.

Venäläinen, A., Lehtonen, I., Laapas, M., Ruosteenoja, K., Tikkanen, O.-P., Viiri, H., Ikonen, V.-P., and Peltola, H.: Climate change induces multiple risks to boreal forests and forestry in Finland: A literature review, Global Change Biology, 26, 4178–4196, https://doi.org/https://doi.org/10.1111/gcb.15183, 2020.

Xu, J., Morris, P. J., Liu, J., and Holden, J.: PEATMAP: Refining estimates of global peatland distribution based on a meta-analysis., University of Leeds. [Dataset], https://doi.org/https://doi.org/10.5518/252, 2017.

Yang, W., Andréasson, J., Phil Graham, L., Olsson, J., Rosberg, J., and Wetterhall, F.: Distribution-based scaling to improve usability of regional climate model projections for hydrological climate change impacts studies, Hydrology Research, 41, 211–229, https://doi.org/10.2166/nh.2010.004, 2010.

Yang, W., Gardelin, M., Olsson, J., and Bosshard, T.: Multi-variable bias correction: application of forest fire risk in present and future climate in Sweden, Natural Hazards and Earth System Sciences, 15, 2037–2057, https://doi.org/10.5194/nhess-15-2037-2015, 2015.

Zhou, N., Hu, X., Byskov, I., Næss, J. S., Wu, Q., Zhao, W., and Cherubini, F.: Overview of recent land cover changes, forest harvest areas, and soil erosion trends in Nordic countries, Geography and Sustainability, 2, 163–174, https://doi.org/https://doi.org/10.1016/j.geosus.2021.07.001, 2021.
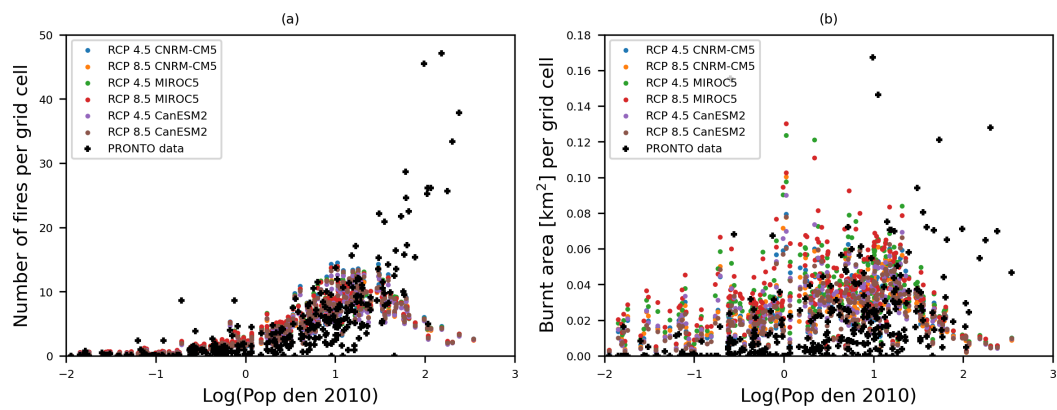
Figure A1. Comparison of results from the SPITFIRE model and observations (Finnish rescue service database PRONTO) for Finland. a) Number of fires in Finland per grid cell and b) burnt area [km^2] in Finland per grid cell as a function of the logarithm of population density in 2010. Annual averages are calculated for the period 1991–2020 for simulations and 2011–2017 for PRONTO data.
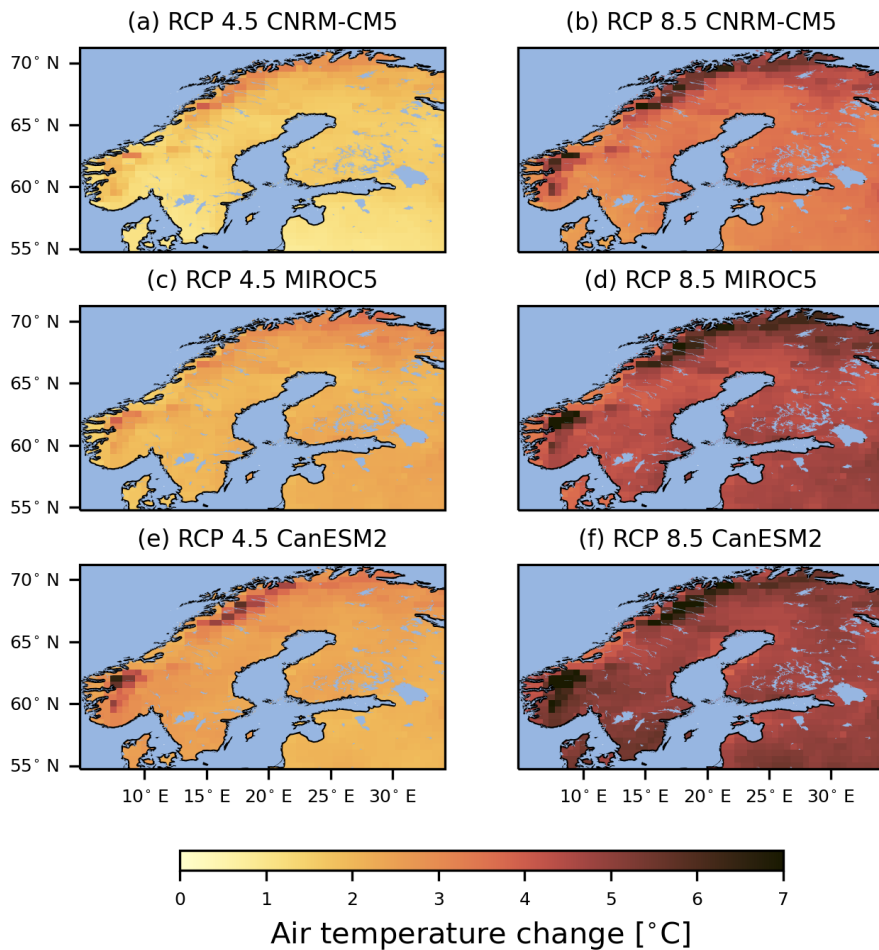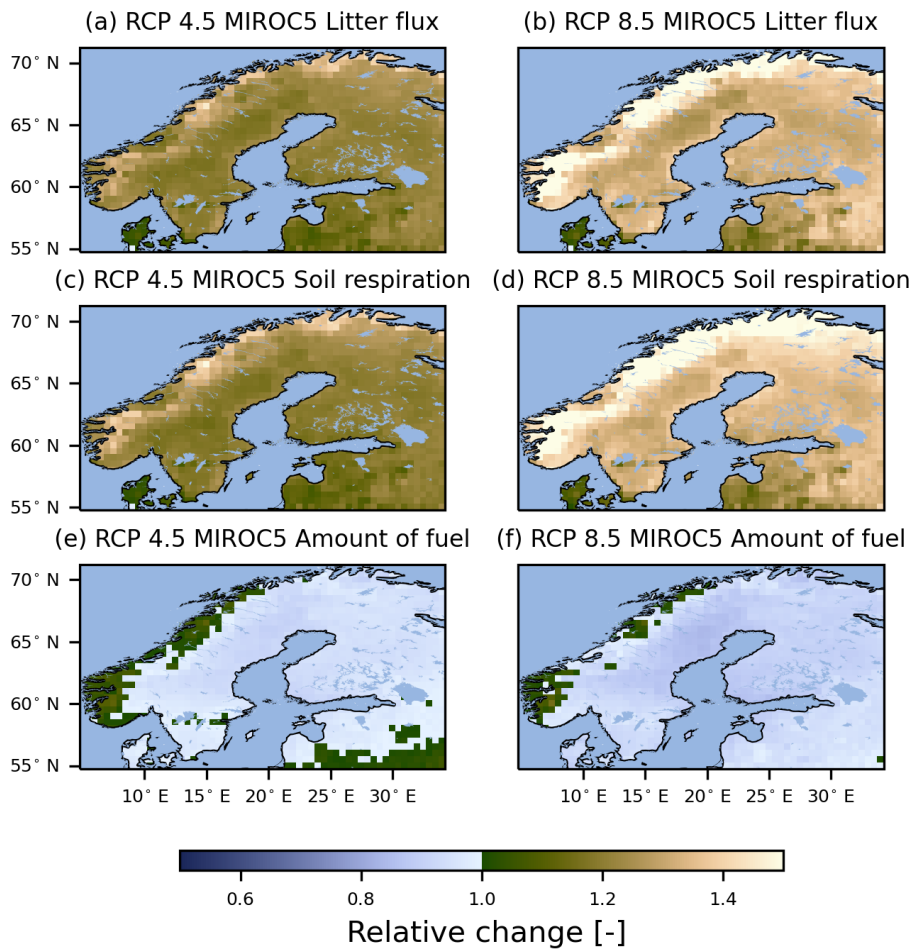
Figure A2. Change in the air temperature [°C] during the summer months (JJA) from the period 1981–2010 to 2071–2100 under two climate change forcing scenarios and three climate global driver models. Yellow indicates around a 1-degree increase, and brown indicates around a 6-degree increase.
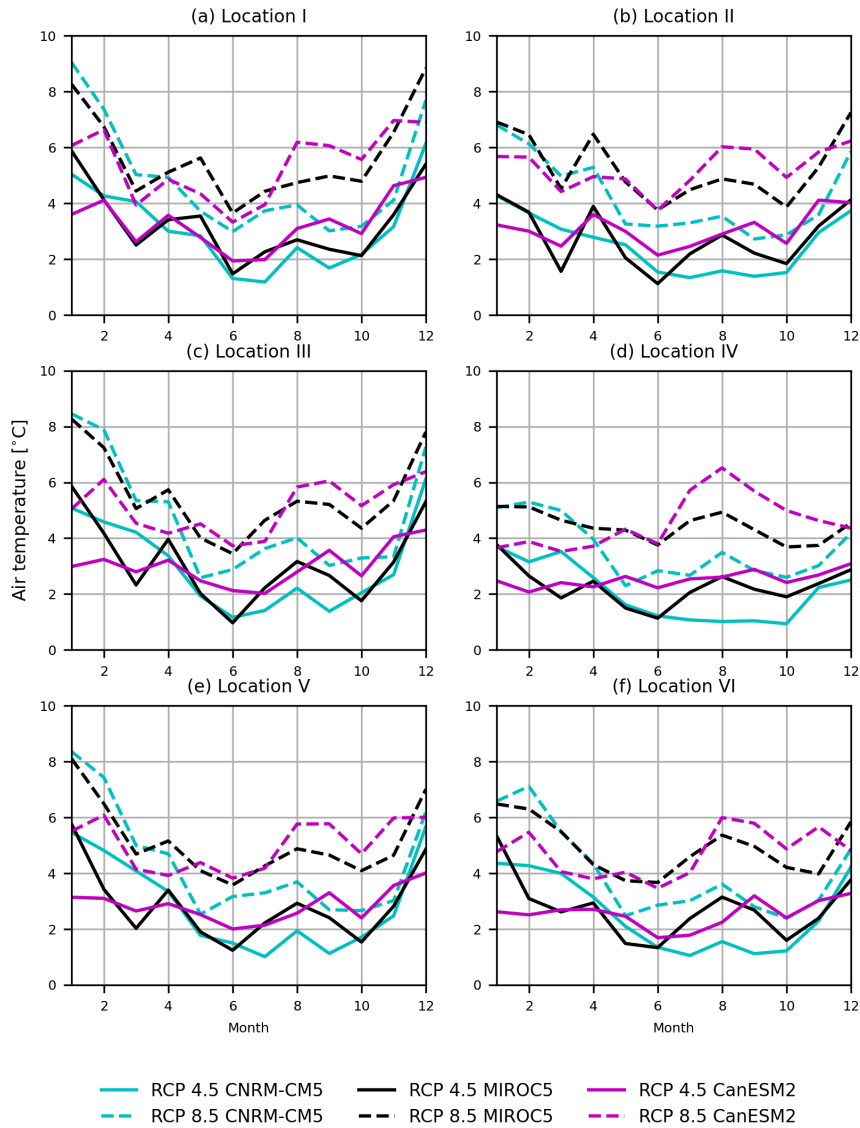
Figure A3. Monthly change from the period 1981–2010 to 2071–2100 in average air temperature [°C] at six locations (See locations from Fig. 1). A positive value indicates an increase in temperature.
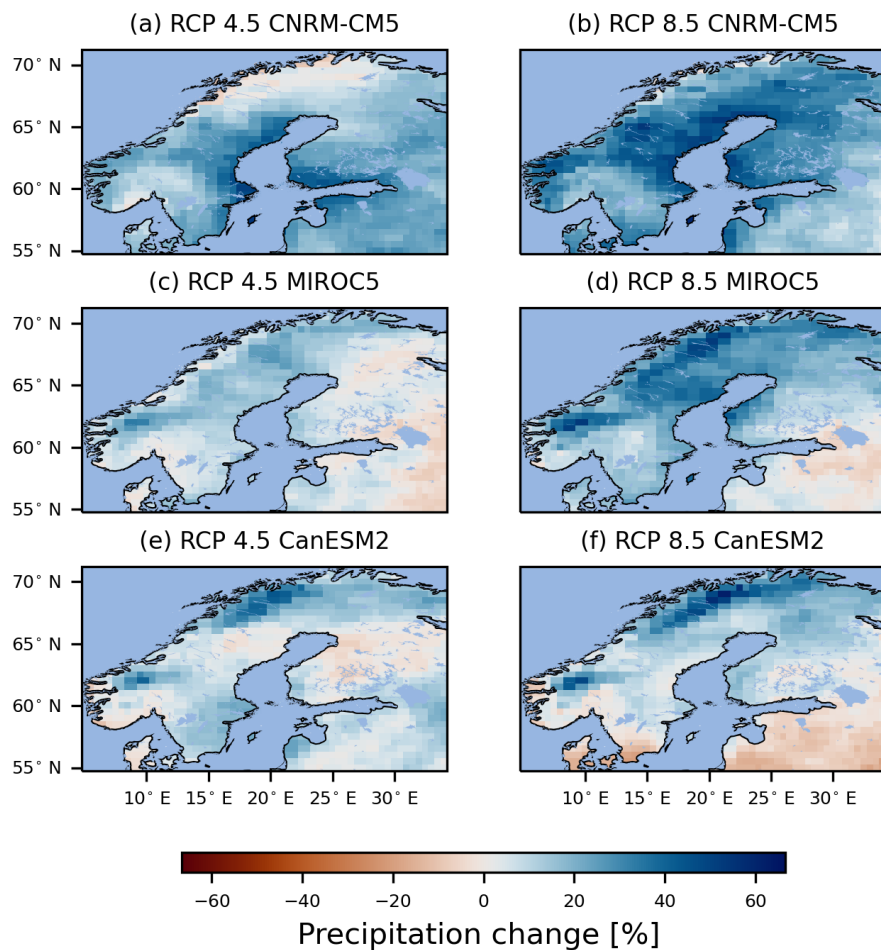
Figure A4. The change in the precipitation [%] during the summer months (JJA) from the period 1981–2010 to 2071–2100 under two climate change forcing scenarios and three global climate driver models. The blue (positive) indicates an increase, and the red (negative) indicates decrease.
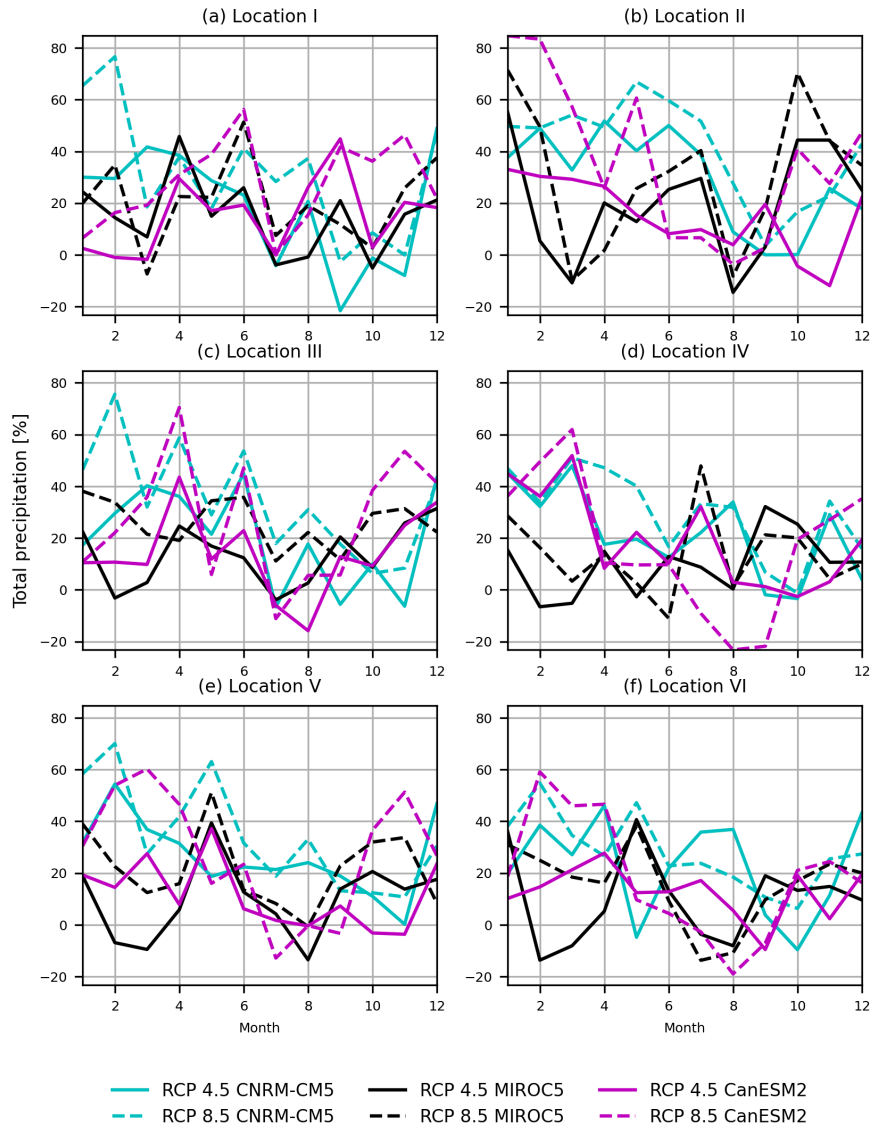
Figure A5. Monthly change from the reference period 1981–2010 to 2071–2100 in average precipitation [%] at six locations (See Fig. 1) A positive value indicates an increase in precipitation.
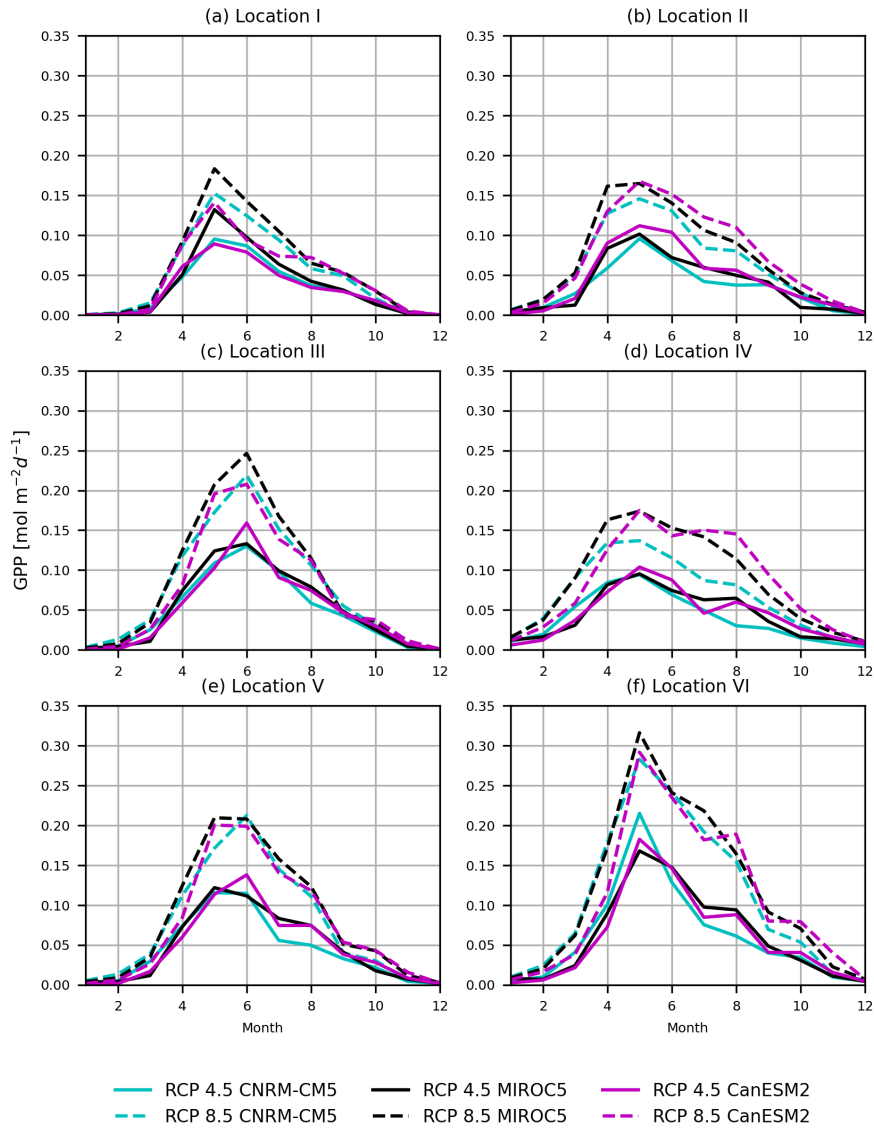
Figure A6. Monthly change from the reference period 1981–2010 to 2071–2100 in average gross primary production (GPP) at six locations. (See Fig. 1) The GPP is summed over all the plant functional types.

Figure A7. Relative change (unitless) in litter flux (a, b), soil respiration (c, d) and amount of fuel (e, f) for the years 2071–2100 compared to the reference period 1981–2010 under two climate change forcing scenarios and the MIROC5 global climate driver model. Less than one (blue) means a decrease, and greater than one (brown) means an increase compared to the reference period.
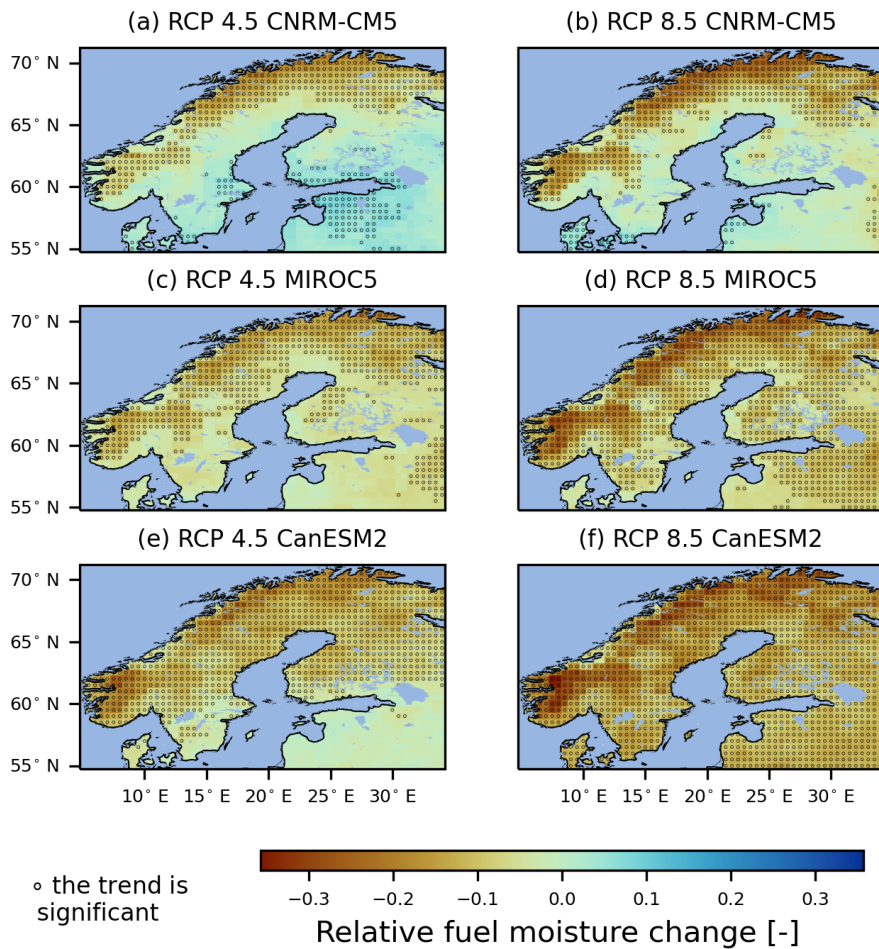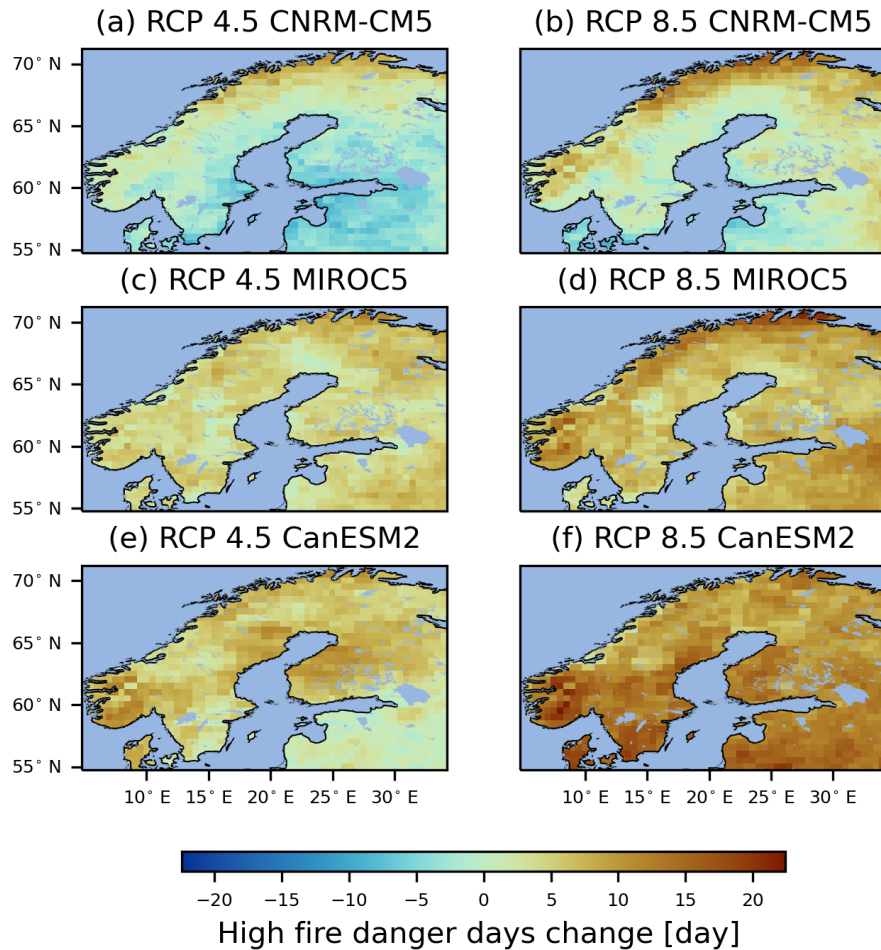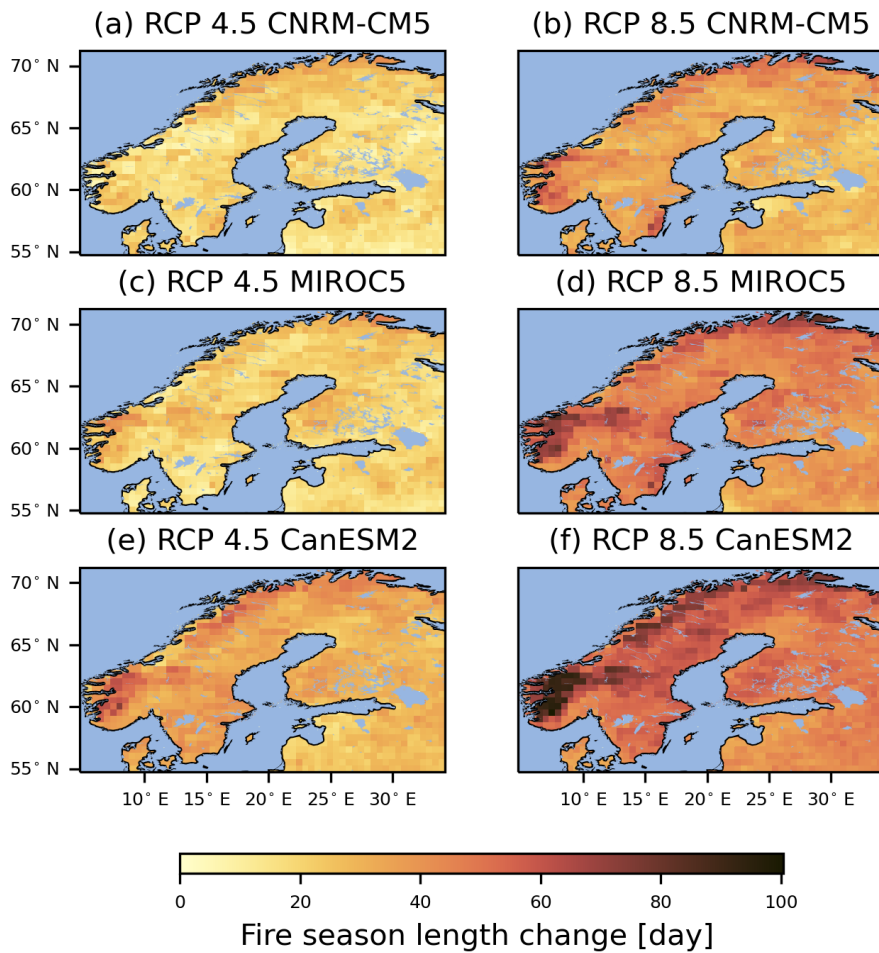
Figure A8. Change of average relative fuel moisture (unitless) for the summer months (JJA) from the reference period 1981–2010 to 2071–2100 under two climate change forcing scenarios and three global climate driver models. Red indicates drier fuel in the future. The dots indicate a significant linear trend according to the Mann-Kendall test (p ≤ 0.05).
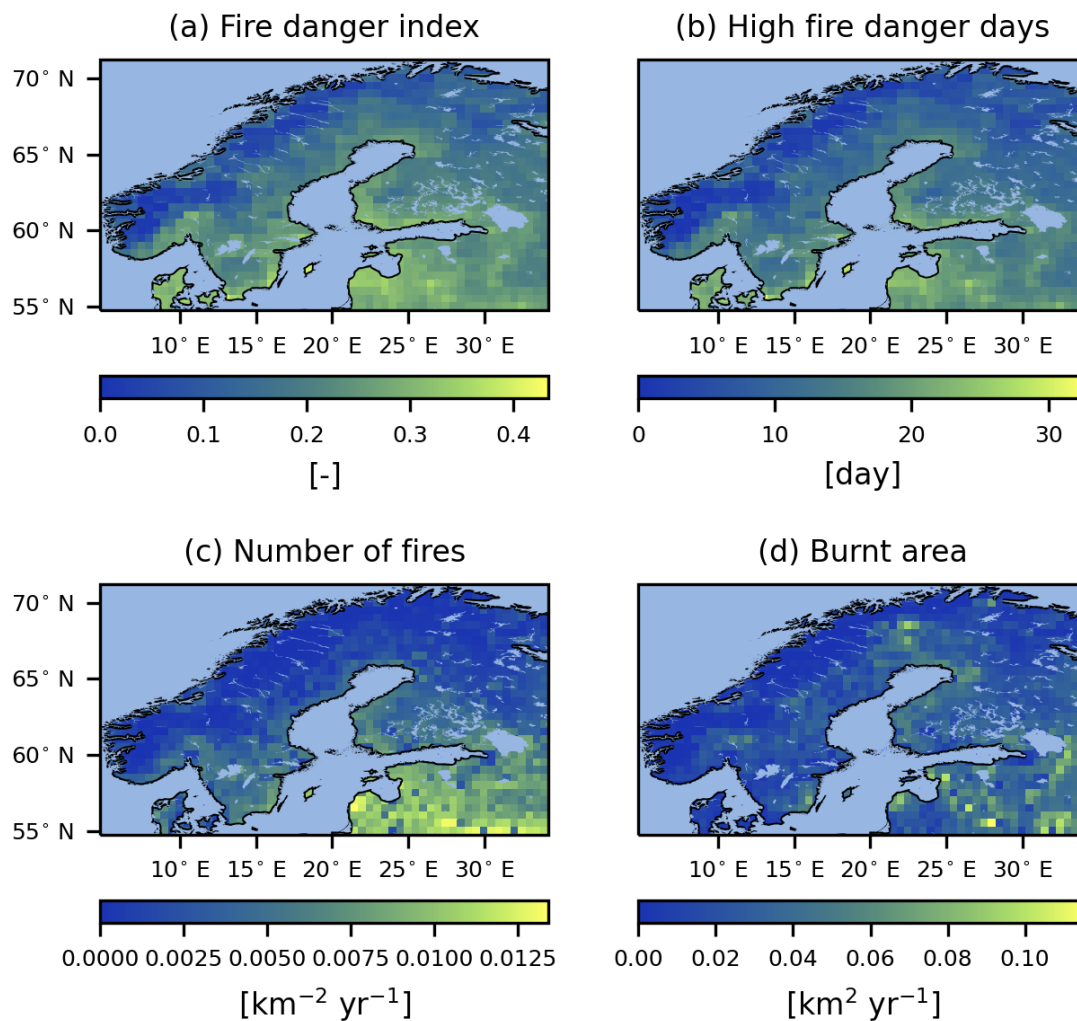
Figure A9. Averages over all the climate projections for summer months a) fire danger index (unitless), b) number of high fire danger days [day] and for annual c) number of fires $[\mathrm{km^{-2}yr^{-1}}]$ and d) burnt area $[\mathrm{km^2yr^{-1}}]$ in the reference period 1981–2010.

Figure A10. Change in the number of very high and extremely high fire danger days [day] from the reference period 1981–2010 to 2071–2100 during the summer months (JJA) under two climate change forcing scenarios and three global climate driver models. Brown indicates an increase in high-fire-risk days.
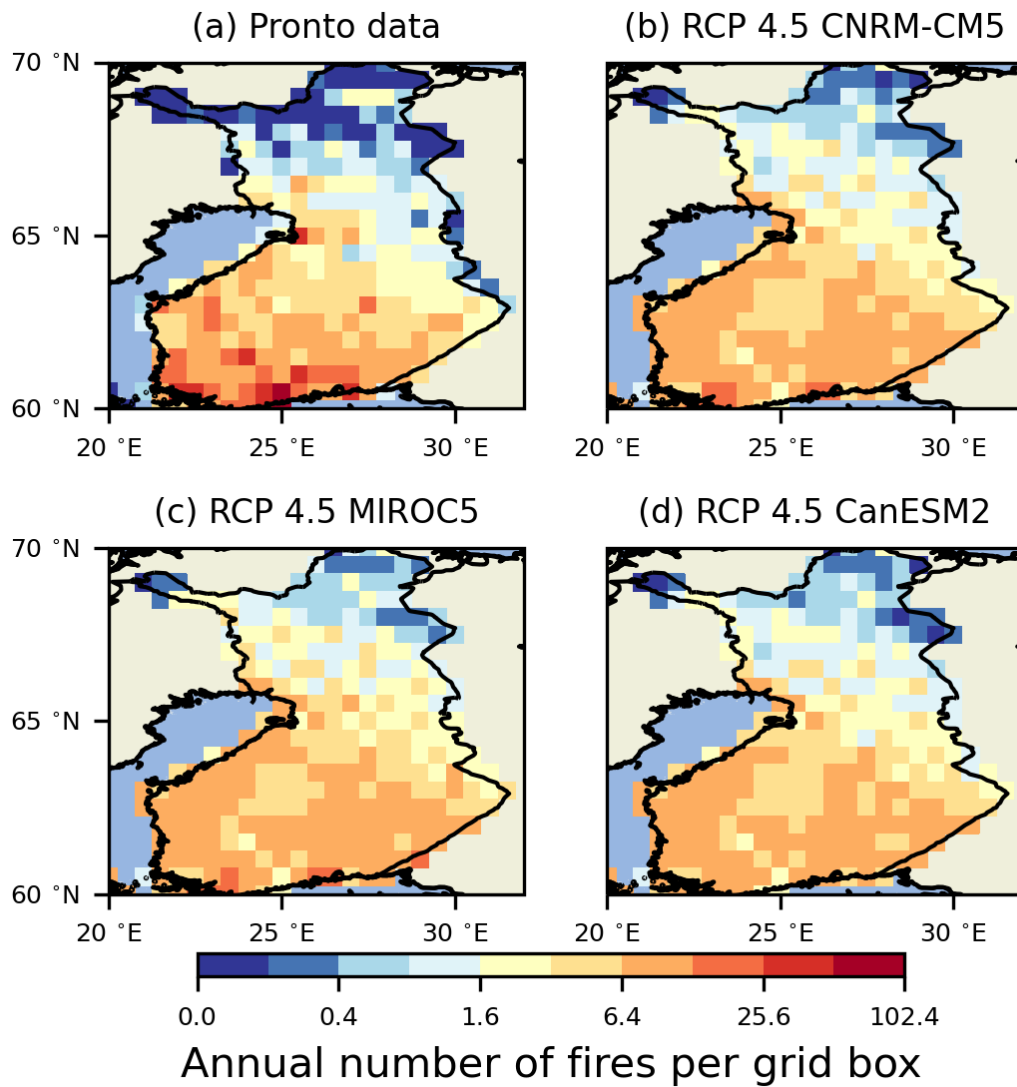
Figure A11. Change in the average length of the fire season [day] from the reference period 1981–2010 to 2071–2100 under two climate change forcing scenarios and three global climate driver models.
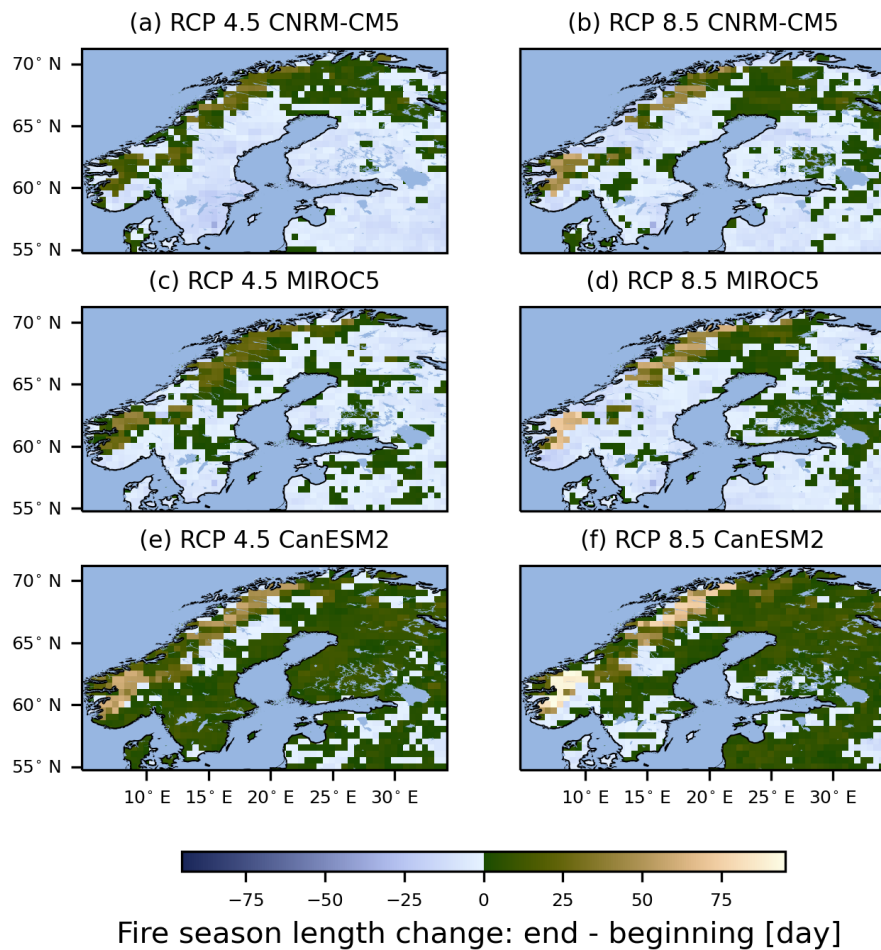
Figure A12. The difference between lengthening at the beginning and end of the fire season [day] from the reference period 1981–2010 to 2071–2100 under two climate change forcing scenarios and three global climate driver models. A negative value (blue) indicates that the fire season is lengthening more at the beginning than at the end of the season.
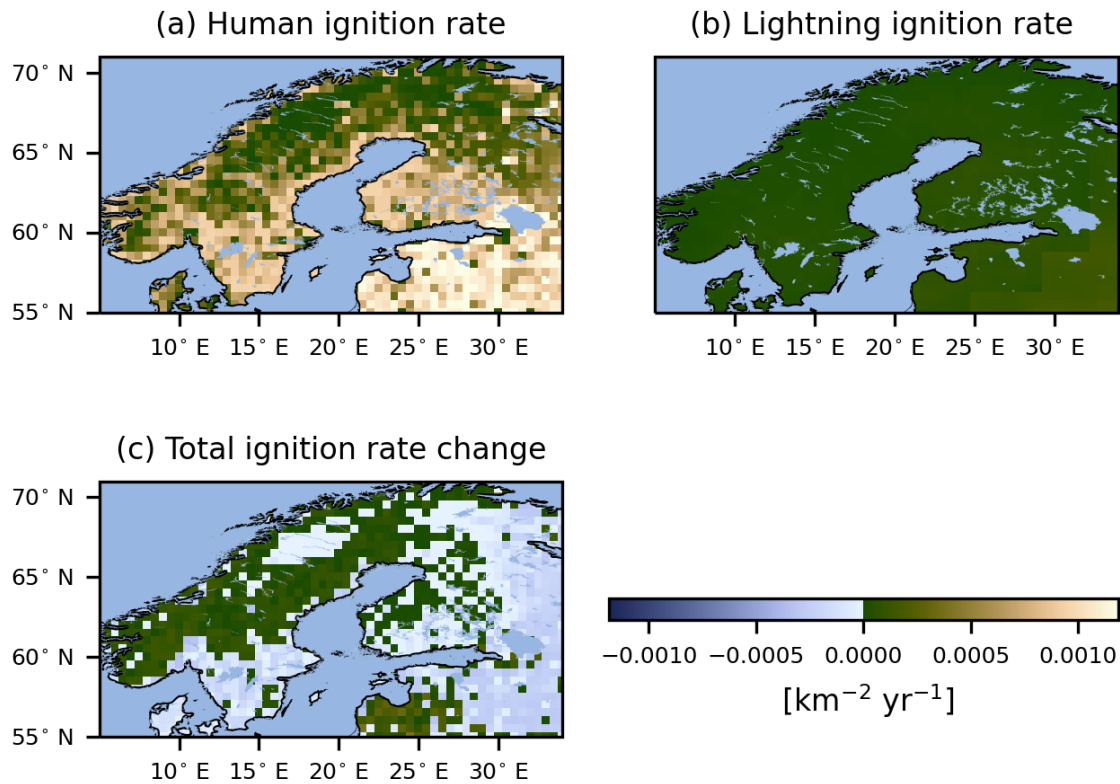
Figure A13. Annual average ignition rate $[\mathrm{km}^{-2}\mathrm{yr}^{-1}]$ caused by a) human or b) lightning in reference period 1981–2010. c) Total ignition rate change from the reference period 1981–2010 to 2071–2100. Light blue indicates less ignitions in the future.

Figure A14. The average number of fires per year in Finland by PRONTO data and RCP 4.5 CNRM-CM5, MIROC5 and CanESM2 on a non-linear scale. Yearly means have been calculated at the period 2011–2018 for PRONTO data and 1991–2020 for simulations.
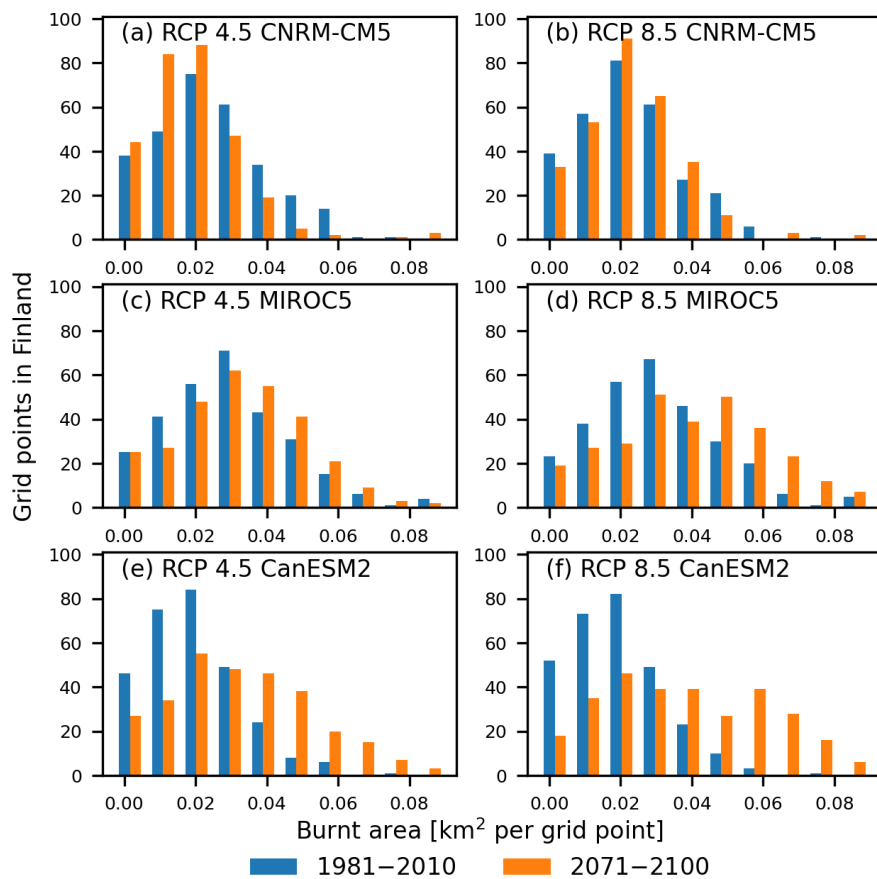
Figure A15. The distribution of annual average burnt areas in 1981–2010 (blue) and 2071–2100 (orange) [km^2 per grid point] in Finland under two climate change forcing scenarios and three global climate driver models.
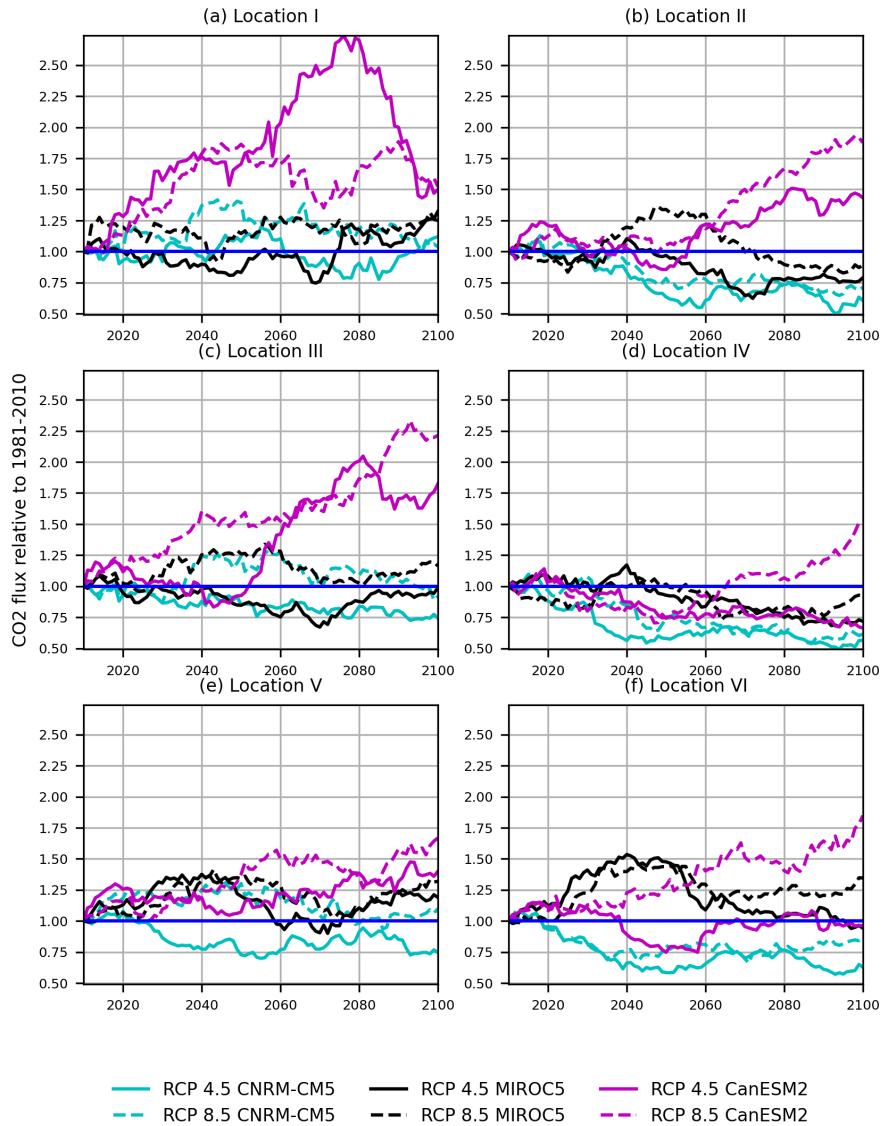
Figure A16. Relative change in CO_2 flux from fires (unitless) from the reference period 1981–2010 to 2071–2100. In each location (Fig. 1 a), the developments under climate change forcing scenario RCP 4.5 (continuous line) and RCP 8.5 (dashed line) are illustrated with the global climate driver models CNRM-CM5 (cyan), MIROC 5 (black) and CanESM2 (magenta). Above one means an increase, below one means a decrease and one means no change compared to the reference period.

Table B1. Average changes from the period 1981–2010 to 2071–2100 and their standard deviations of the start day, the end day and the length of the fire season in six locations (See Fig. 1) under two climate change forcing scenarios and three global climate driver models.

Location	Climate projection	Change in the start day (std) [day]	Change in the end day (std) [day]	Change in the length of fire season (std) [day]
I 67° N 26° E Northern Finland	RCP 4.5 CNRM-CM5	-9.8 (26.1)	13.0 (24.6)	22.8 (33.3)
	RCP 4.5 MIROC5	-13.0 (30.0)	10.0 (28.0)	23.0 (43.2)
	RCP 4.5 CanESM2	-8.4 (27.2)	15.4 (26.9)	23.8 (37.6)
	RCP 8.5 CNRM-CM5	-12.4 (23.8)	20.3 (26.5)	32.6 (36.1)
	RCP 8.5 MIROC5	-17.7 (33.1)	23.9 (22.6)	41.6 (37.1)
	RCP 8.5 CanESM2	-14.9 (29.7)	24.9 (26.9)	39.8 (43.9)
II 62° N 16° E Central Sweden	RCP 4.5 CNRM-CM5	-12.0 (29.1)	4.6 (29.5)	16.6 (41.9)
	RCP 4.5 MIROC5	-15.7 (31.9)	9.8 (22.2)	25.5 (41.5)
	RCP 4.5 CanESM2	-16.6 (26.2)	23.0 (29.8)	39.6 (38.9)
	RCP 8.5 CNRM-CM5	-15.3 (31.2)	16.9 (28.3)	32.2 (44.7)
	RCP 8.5 MIROC5	-30.9 (27.7)	20.9 (23.1)	51.9 (37.2)
	RCP 8.5 CanESM2	-25.9 (26.5)	33.2 (28.3)	59.1 (39.0)
III 64° N 25° E Central Finland	RCP 4.5 CNRM-CM5	-15.5 (31.1)	6.5 (33.4)	22.0 (49.4)
	RCP 4.5 MIROC5	-20.0 (31.0)	14.7 (26.7)	34.8 (43.0)
	RCP 4.5 CanESM2	-12.0 (28.7)	24.3 (26.3)	36.3 (36.6)
	RCP 8.5 CNRM-CM5	-22.1 (26.0)	9.3 (29.5)	31.4 (41.6)
	RCP 8.5 MIROC5	-26.8 (31.4)	23.0 (28.4)	49.8 (46.6)
	RCP 8.5 CanESM2	-22.0 (25.2)	33.1 (25.7)	55.2 (33.7)
IV 57° N 15° E Southern Sweden	RCP 4.5 CNRM-CM5	-19.5 (37.7)	2.3 (32.8)	21.7 (43.6)
	RCP 4.5 MIROC5	-8.4 (32.6)	2.3 (23.7)	10.7 (34.1)
	RCP 4.5 CanESM2	-17.0 (29.4)	24.5 (31.3)	41.5 (35.7)
	RCP 8.5 CNRM-CM5	-21.8 (39.3)	17.0 (32.9)	38.8 (50.6)
	RCP 8.5 MIROC5	-32.4 (31.6)	19.8 (34.5)	52.2 (48.3)
	RCP 8.5 CanESM2	-26.2 (28.0)	23.4 (26.6)	49.7 (35.8)
V 62° N 28° E Southern Finland	RCP 4.5 CNRM-CM5	-7.6 (27.9)	8.8 (29.9)	16.4 (41.4)
	RCP 4.5 MIROC5	-6.8 (24.7)	10.5 (24.4)	17.3 (36.4)
	RCP 4.5 CanESM2	-9.4 (25.9)	18.8 (25.1)	28.1 (39.2)
	RCP 8.5 CNRM-CM5	-7.0 (26.0)	16.0 (29.1)	23.0 (45.2)
	RCP 8.5 MIROC5	-19.4 (22.0)	25.0 (23.7)	44.4 (33.1)
	RCP 8.5 CanESM2	-21.5 (25.6)	27.4 (27.0)	48.8 (35.4)
VI 59° N 27° E Estonia	RCP 4.5 CNRM-CM5	-17.7 (32.2)	7.2 (31.7)	24.8 (44.9)
	RCP 4.5 MIROC5	-12.8 (30.8)	11.6 (32.6)	24.4 (38.2)
	RCP 4.5 CanESM2	-12.3 (27.4)	11.9 (29.9)	24.3 (44.8)
	RCP 8.5 CNRM-CM5	-19.1 (34.3)	9.4 (30.9)	28.5 (49.5)
	RCP 8.5 MIROC5	-25.0 (29.1)	18.8 (26.3)	43.8 (37.8)
	RCP 8.5 CanESM2	-16.5 (25.1)	21.6 (35.7)	38.1 (48.5)